ELECTON-IMPACT STUDIES

USING THE HITACHI RMU 6-D

MASS SPECTROMETER

by David F. Torgerson

A Thesis Presented To The
Faculty Of Graduate Studies
Of The University Of Manitoba
In Partial Fulfilment Of
The Degree Of

MASTER OF SCIENCE

From the Chemistry Department
University of Manitoba
Winnipeg, Manitoba

September, 1966

ACKNOWLEDGEMENTS

I wish to thank Dr. J. B. Westmore, my research supervisor, for his perpetual optimism, patience, and advice - all of which, it is hoped, are manifested into this thesis.

I should also like to thank Mr. Les Wilkins for the construction of valuable equipment and Dr. D. McBride for his interest and for the method of preparation of PF_3.

To My Parents

TABLE OF CONTENTS

INTRODUCTION

APPARATUS AND PROCEDURE

THE ELECTRON-IMPACT STUDY OF PF_3

ILLUSTRATION INDEX

ILLUSTRATION INDEX (CONTINUED)

TABLE INDEX

ABSTRACT

The Hitachi RMU 6-D mass spectrometer was studied in order to determine the optimum conditions for the measurement of ionization efficiency curves. These conditions were then applied to the electron-impact study of phosphorus trifluoride from which nine positive ions (PF_3^+, PF_2^+, PF^+, P^+, F^+, P^{++}, PF^{++}, PF_2^{++}, PF_3^{++}) and one negative ion (F^-) were observed. The ionization efficiency curves were determined for all the ions except P^{++}, and the appearance potentials were measured along with heats of formation. The ionization potential of PF_3 was measured using three different procedures and was found to be 11.63 ± 0.02 electron volts. The fragmentation reactions are discussed and upper limits on the ionization potentials of PF_2 and PF are found.

INTRODUCTION

PART ONE: GENERAL INTRODUCTION

A. PRINCIPLE OF THE DIRECTION-FOCUSING MASS SPECTROMETER

Direction-focusing mass spectrometry denotes the method of analysis in which ions formed by the electron bombardment (or photo-ionization) of a sample are accelerated in an electric field and subsequently dispersed by a magnetic field into a number of beams, each with a specific mass to charge ratio (m/e). The ion beams are in turn focused onto a fixed collector where they are detected electrically with further amplification. The plot of the relative intensities of these beams against their mass to charge values constitutes a mass spectrum.

B. IONS FORMED FROM ELECTRON-IMPACT

The ionization of the gaseous sample is carried out, in most cases, by the bombardment of the sample with low energy electrons. As the ionizing electron beam is usually accelerated through about 70 volts and as first ionization potentials rarely exceed 15 electron volts, much of the excess energy, besides being dissipated as kinetic energy, is absorbed into the vibrational modes of the molecule and unimolecular dissociation results. Accordingly, several different processes will be taking place to produce the various ions making up the mass spectrum (or "pattern coefficient") of a compound. The most common of these processes will now be considered:

(a) Parent Ions

These are produced by the removal of a single electron from the atomic or molecular species admitted to the ion source. In general,

The reaction may be denoted as

$$M + e = M^+ + 2e.$$

The m/e value of the ion, therefore, gives the molecular weight of the compound.

(b) Multiply-Charged Ions

If the electron beam is sufficiently energetic such that it exceeds the second (or greater) ionization potential, then doubly-charged ions result:

$$M + e = M^{++} + 3e.$$

It should be noted, however, that the probability of the secondary ionization process

$$M^+ + e = M^{++} + 2e$$

to form doubly-charged ions is slight, due to the relatively low concentration of M^+ ions in the ion source.

(c) Fragment Ions

Various bond-dissociation processes that may take place during the electron bombardment of the parent species lead to the formation of fragment ions. These processes, as previously noted, arise from the excess energy contained in the parent's vibrational and electronic degrees of freedom. An illustrative example for hydrocarbons is n-butane (see figure 1) which, by one process, can dissociate to form an ion and a neutral atom:

$$C_4H_{10} + e = C_4H_9^+ + H + 2e.$$

FIGURE ONE

THE MASS SPECTRUM OF N-BUTANE

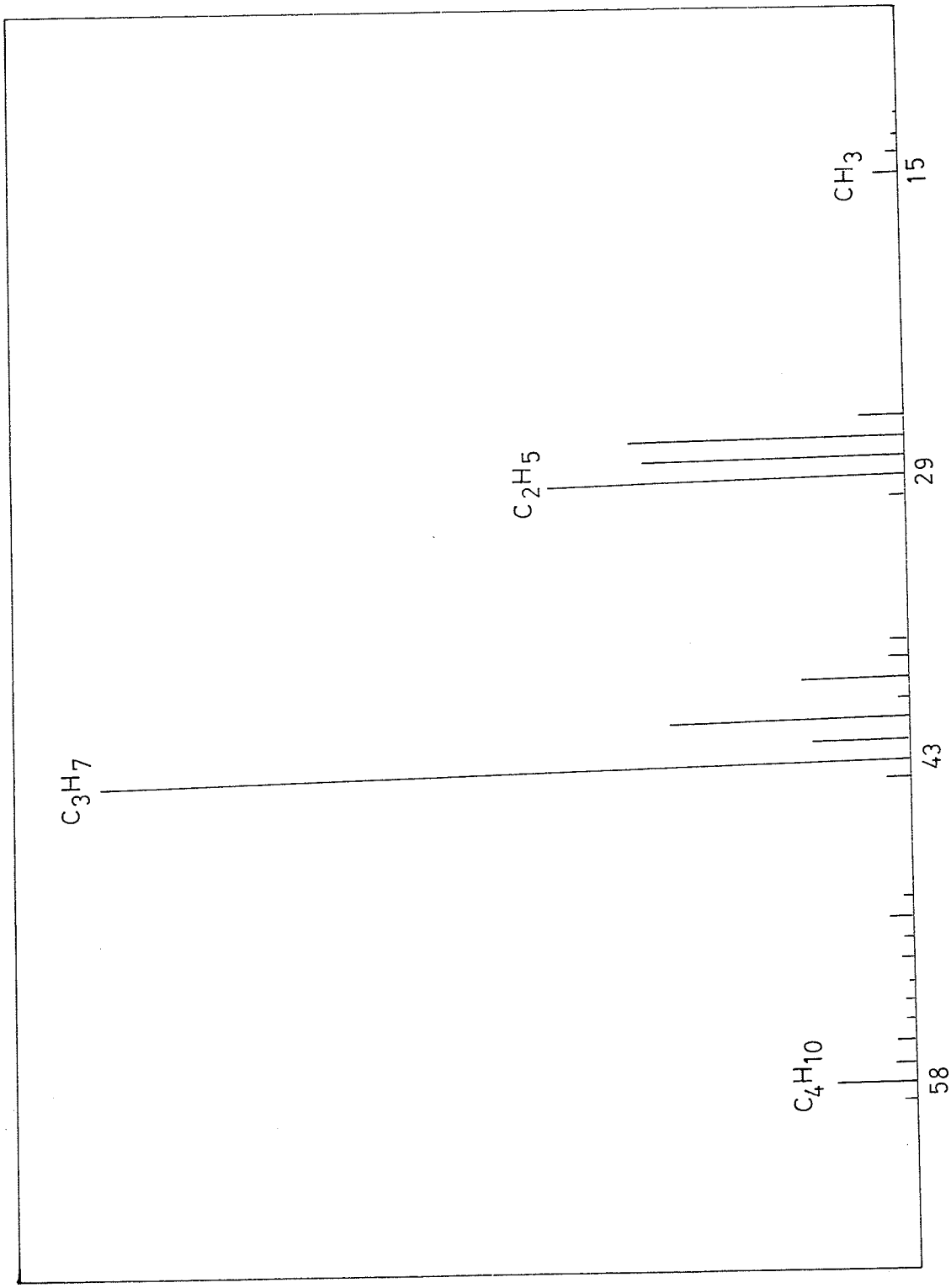
C_3H_7
43
C_2H_5
29
CH_3
15
C_4H_{10}
58

(d) Metastable Ions

If an ion is formed in the ion source with excess energy in its vibrational modes, it may not at once dissociate if its rate of decomposition is slow. In terms of Slater's theory[1] this time lag may be interpreted as the time required for a number of vibrations within the molecule to come into phase. Therefore, the ions will be accelerated towards the magnetic field, dissociating outside the ion source into smaller neutral species and new positively-charged ions. These new ions have been given the name "metastable ions" in order to specify that they originate from unstable ions and not from a primary electron-impact process. The products of these metastable transitions reach the collector along with other ions of different masses but are observed neither at their "original" mass nor at their "new" mass. Most often, in fact, metastable transitions occur in the mass spectrum at non-integral mass numbers as illustrated in figure 2 for n-butane. The 25.1, 30.4, and 31.9 peaks correspond respectively to the metastable transitions:[2]

$$[29]^+ = [27]^+ + [2]$$
$$[58]^+ = [42]^+ + [16]$$
$$[58]^+ = [43]^+ + [15].$$

Figure 2 also serves to illustrate the fact that metastable ion intensities are quite weak and are observed clearly only at higher detection sensitivities.

J. A. Hipple, R. E. Fox, and E. U. Condon[3] have developed a simple relation for the position of metastable peaks in the mass spectrum. If M_o^x is the mass of the "metastable" ion formed from the dis-

FIGURE TWO

DETAIL OF THE MASS SPECTRUM OF N-BUTANE
SHOWING METASTABLE PEAKS AT M/E VALUES
25.1, 30.4, AND 31.9

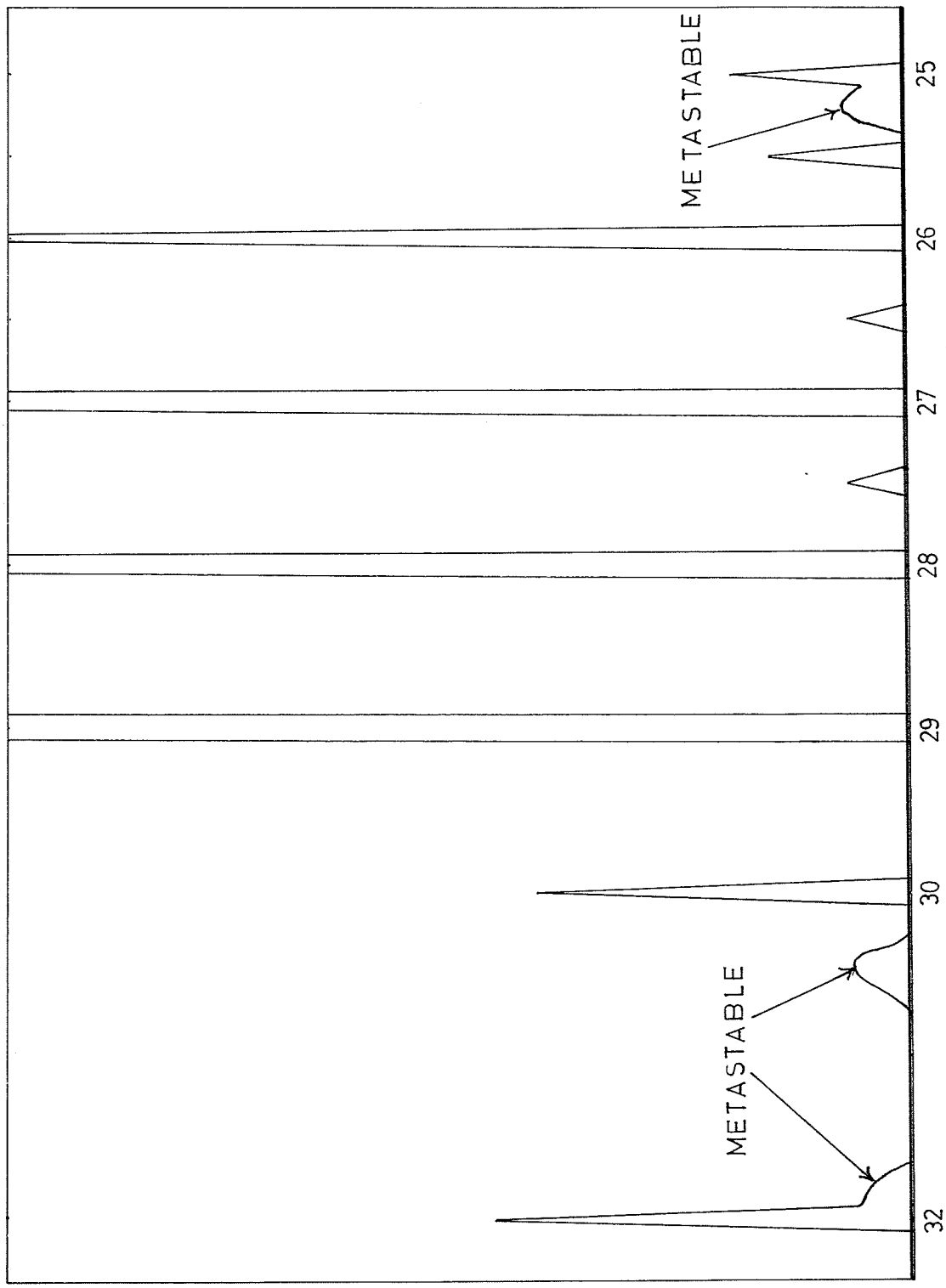
METASTABLE
METASTABLE
25
26
27
28
29
30
32

sociation of an unstable primary ion of mass M_o, then the m/e value, M, at which the metastable ion will be observed is given by

$$M = [M_o^*]^2/[M_o].$$

(e) Rearrangement Ions

At the point of unimolecular dissociation of the parent compound, rearrangements may take place in the molecule producing rearranged fragments. This produces peaks in the mass spectrum that cannot be accounted for by a simple bond-cleavage mechanism. An example of such a process is the formation of $[CH_2D]^+$ ions in the electron-impact study of 1,1,1-trideuteroethane[4].

(f) Negative Ions

There are two principal mechanisms by which negative ions may be produced by electron-impact:

(1) electron capture: $AB + e = AB^- = A + B^-$, and

(2) ion-pair production: $AB + e = A^+ + B^- + e$.

These ions can be detected by reversing the ion-optics of the mass spectrometer; however, measurements are difficult to carry out as negative ions are almost always formed with initial kinetic energy and as their intensities are usually much smaller than those for positive ions.

(g) Ion-Molecule Reactions

As the electron beam is accelerated through a narrow path in the ion source, it is apparent that only a fraction of the gaseous sample will become ionized. This leads to various secondary processes involving reactions between primary ions and neutral molecules. These secondary interactions yield products that tend to complicate the mass spectrum of a sample. An example is the appearance of the hydronium

Figure 3 shows the Morse electronic potential curves for a diatomic molecule (or in general, for one of the possible modes of vibration of a polyatomic molecule) in its ground state AB and in its first ionic excited state AB^+. The potential functions are not parabolic, as expected for simple harmonic motion, but rise rapidly as the nuclei approach, while for larger separations the molecule dissociates. As the potential function will depend on the electronic state of the molecule, it is possible that the equilibrium internuclear distance will differ in the upper electronic state from its value in the ground state.

From the classical picture of vibrational motion, the nuclei would be expected to spend most of the time at the extremes of their motion with very small or zero momentum. Quantum mechanically, if the Schrodinger wave equation is solved for ϕ, the wave function for vibrational states, then the probability of position of the nuclei is proportional to $|\phi|^2$ (7). Plotting $|\phi|^2$ for the first few vibrational levels, it is apparent that for the ground state the maximum probability occurs at the centre of the potential curve, while for the excited states, the maximum falls near the extremes of the classical limits:

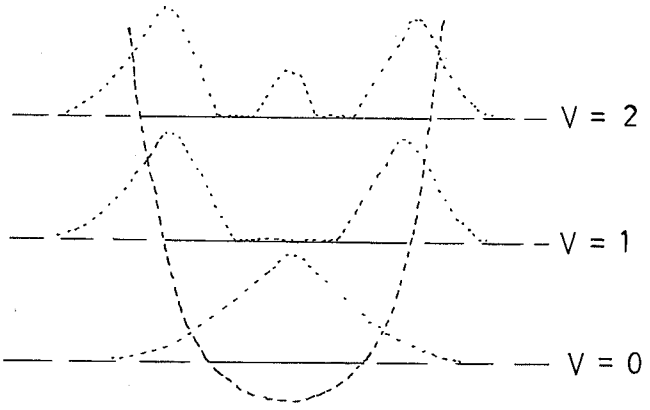

FIGURE THREE

POSSIBLE FRANCK-CONDON TRANSITIONS FOR
THE DIATOMIC MOLECULE CASE AS A RESULT
OF ELECTRON-IMPACT

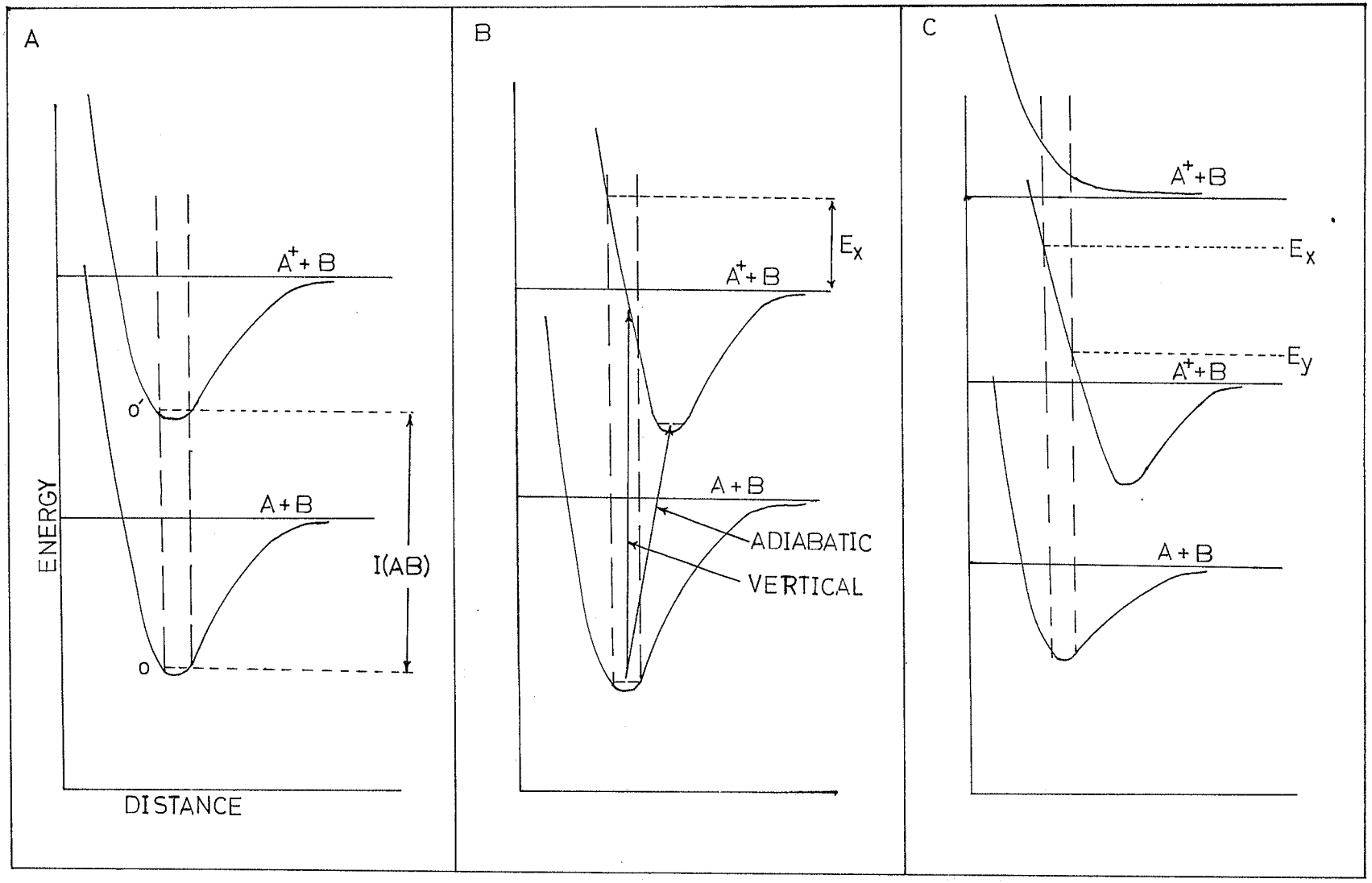

FIGURE 3

And therefore, as these are the most probable positions of the nuclei, it follows that electronic transitions will most likely occur from these points on the potential curves.

Applying the Franck-Condon Principle to these transitions, two restrictions will now arise: (1) As the transition must take place such that the AB internuclear distance equals the AB^+ internuclear distance, the transitions must be represented by a vertical line. (2) Since the molecule must go to a point on the upper electronic state curve where the momentum is small or zero, the transition is most likely to end at either of the extremes of a vibrational level (or at the centre of the lowest level).

Considering figure 3-A, the upper electronic state function is not appreciably displaced from the ground one. Consequently, all transitions lead to the formation of AB^+ molecules in their ground electronic state with some vibrational exitation. The ionization potential, defined as the energy required to remove an electron from the highest occupied molecular orbital of the molecule in its ground state, is given by the 0-0' transition which, from figure 4-D, is also the most probable one. As no dissociation occurs, there is no excess kinetic energy due to fragments (figure 4-G).

Part of the continuum may be included in the transitions as indicated in figure 3-B. Under these conditions dissociation fragments of AB will be formed as well as vibrationally excited AB^+ molecules. It is convenient at this time to differentiate between the <u>adiabatic</u> ionization potential and the <u>vertical</u> ionization potential. The former is strictly defined as the energy required for the 0-0' transition while the latter represents the energy required for the vertical 0-V' transition, where V' is the vibrational quantum number for

FIGURE FOUR

TRANSITION PROBABILITIES
AND
KINETIC ENERGY DISTRIBUTIONS OF PRODUCTS
FOR FRANCK-CONDON TRANSITIONS

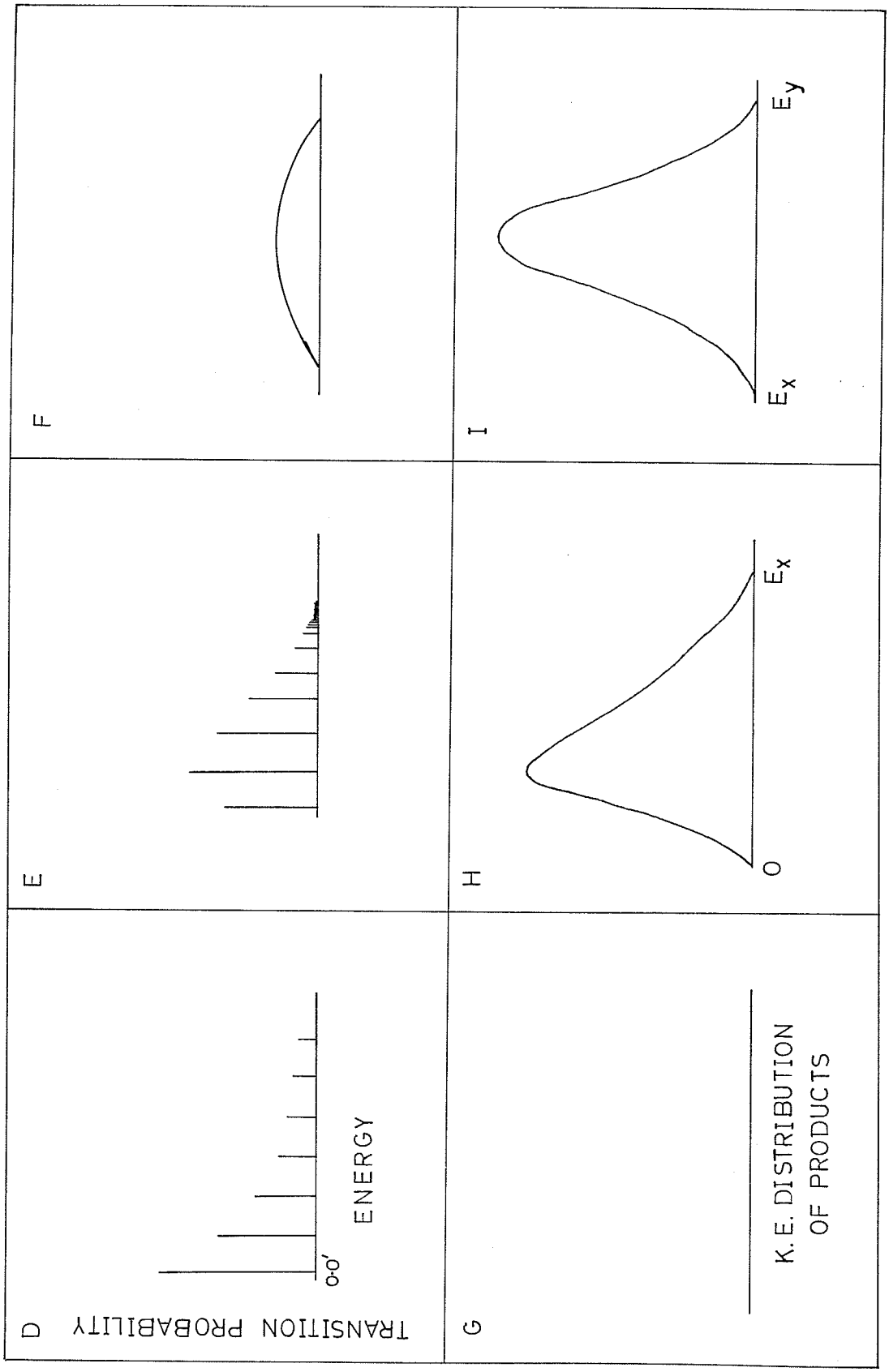
D
TRANSITION PROBABILITY
o-o'
ENERGY
E
F
G
K.E. DISTRIBUTION
OF PRODUCTS
H
O
E_x
I
E_x
E_y

FIGURE 4

an excited vibrational state of the AB^+ molecule. These are illustrated in figure 3-B.

Figures 4-E and 4-H give the transition probabilities and the kinetic energy distributions of the fragments respectively. The kinetic energy of the products will vary from 0 to E_x, where E_x is the maximum energy above the dissociation energy of AB^+ that the transition in figure 3-B can impart to a fragment.

Finally, as indicated in figure 3-C, the internuclear distance may be shifted so far in the AB^+ molecule that all transitions lie in the continuum. A further case, also shown in figure 3-C, which is analogous to this one occurs when AB^+ does not have a stable electronic state. Therefore, all transitions will lead to fragments of AB with kinetic energies lying between E_x and E_y, the maximum and minimum energies respectively at which the vertical transition intersects the AB^+ electronic state function (figure 4-I).

PART TWO: IONIZATION EFFICIENCY CURVES

A. INTRODUCTION

An ionization efficiency curve is the plot of the ion intensity or ion current for a particular m/e peak in a mass spectrum against the energy of the bombarding electrons. Figure 5 is the ionization efficiency plot for Kr^+ as determined by the Hitachi RMU 6-D mass spectrometer. This curve is typical for most species, the ion current rising linearly with increasing electron acceleration voltage and passing through a maximum in the 30 to 50 volt region. At very high electron voltages (thousands of e.v.), the probability that an electron will produce an ion which reaches the collector is a small fraction of that for the 70 volt range (8). Consequently, there is a slight drop in the ion current as the voltage is increased above the maximum point in the curve. However, as figure 5 serves to illustrate, the change in ion intensity in the 50 volt region is much less than the change on the linearly rising portion of the curve. For analytical purposes, therefore, the electron acceleration voltage is usually set at either 50 or 70 volts, where slight variations in voltage will not be as likely to affect the reproducibility of the results.

A salient feature of the curve in figure 5 is the "foot" or "tail" at the base of the plot. This is primarily caused by the inherent energy spread in the bombarding electrons. The spread in energy is due to the Maxwellian distribution in the energy of electrons being emitted from a hot filament. A second reason for the "foot" is that in some cases excited vibrational states in the molecule are

FIGURE FIVE

IONIZATION EFFICIENCY CURVE
FOR Kr^+
(UNCORRECTED ENERGY SCALE)

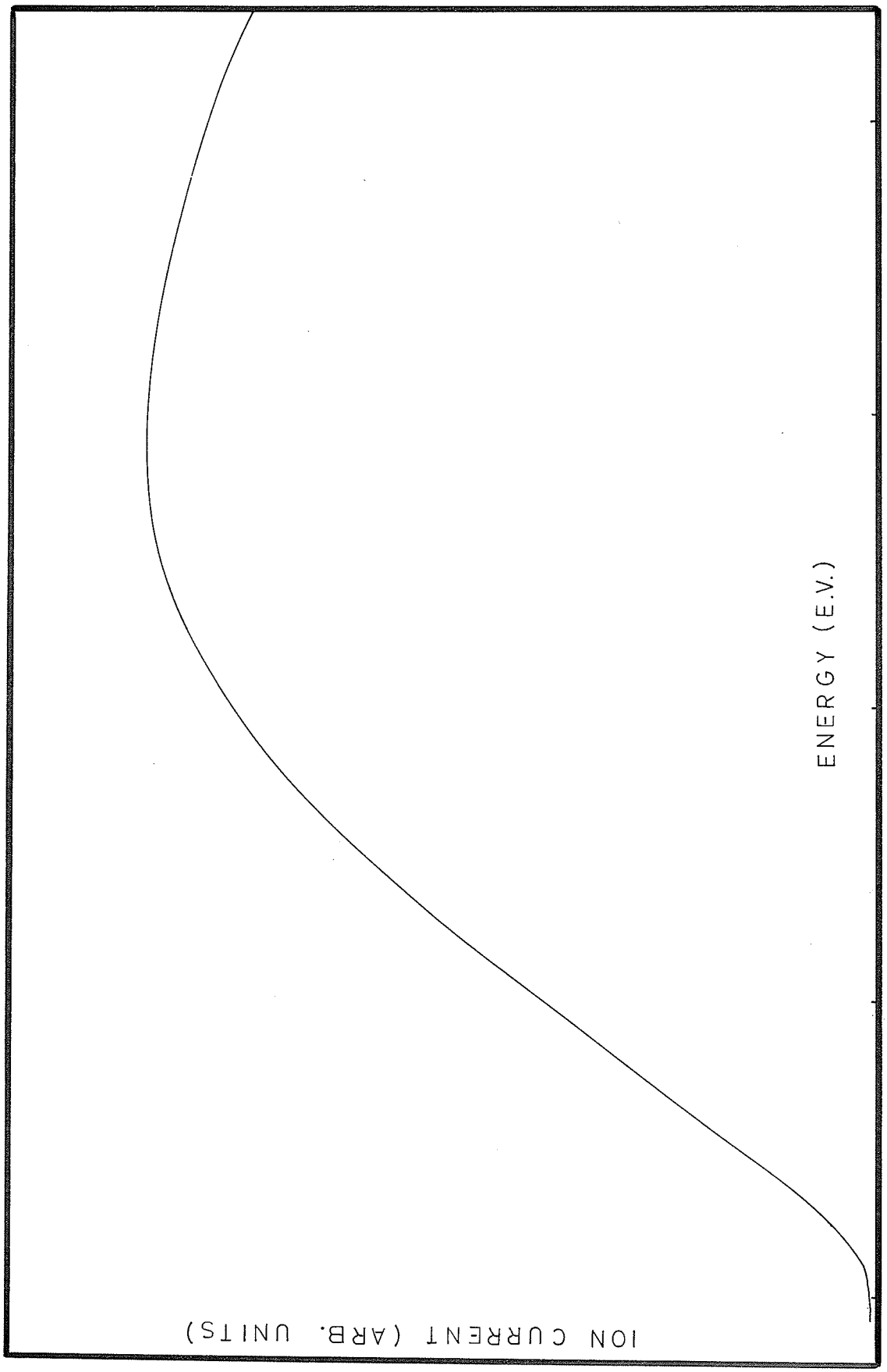
ION CURRENT (ARB. UNITS)
ENERGY (E.V.)
10
20
30
40
50

close in energy to the ground state. If these excited states happen to be thermally populated, electronic transitions will take place from them at lower electron energies than for the ground state transitions. Broadly speaking, however, the energy spread in the ionizing electron beam is by far the principal cause of the "foot" in the curve.

Honig(9) has attempted a theoretical analysis of ionization efficiency curves. Assuming the electron energy spread is Maxwellian and that all electrons with thermal energies larger than the work function ϕ, the energy barrier an electron must overcome to be emitted from the surface of a metal, leave the filament, then the number of electrons, $dNe(U)$, with thermal energies between U and U + dU leaving the filament per second is given by

$$dNe(U) = (4\pi mA/h^3) \cdot U \cdot \exp[-(\phi + U)/kT]dU \qquad (I)$$

where m = electron mass in grams, A = filament surface area in cm^2, h and k are respectively the Planck and Boltzmann constants, and T = absolute temperature of the filament. As the electrons pass through an electrostatic field V before reaching the ionizing region, their total energy will be E = U + V. The total number of ions produced per second that ultimately reach the collector, Ni(V), formed by an electron accelerating potential of V volts, is given by

$$Ni(V) = \int_0^E Ne(U)p(E)dE \qquad (II)$$

where p(E) is the probability (or more strictly, the "probability density") that an electron with total energy E produces an ion that reaches the collector.

The appearance potential or critical voltage, Vc, is defined as the minimum electron energy required for a particular ion just to be formed from the neutral species. However, due to the "foot" of the ionization efficiency curve, which tends to extend the plot to energies below the appearance potential, the actual point corresponding to the onset of ionization cannot be accurately determined without further analysis of the curve.

It has been found empirically that p(E) is related to the "excess energy" of the electrons above the appearance potential, Vc: (10)

$$\begin{aligned} p(E) &= 0 && \text{for } E \leqslant Vc \\ p(E) &= C(E - Vc)^n && \text{for } E > Vc \end{aligned} \qquad \text{(III)}$$

where n and C are constants. Honig(9) found empirically that the best value of n is 2, although the relation between p(E) and (E - Vc) is now considered to be linear for most cases(8,10). On substituting equations I and III into equation II and carrying out the integration (using n = 2), then the following expressions for the ion current, Ni(V), arise:

$$Ni(V) = 2C'kT^3[Vc - V + 3kT]\cdot\exp[-(\phi + Vc - V)/kT] \qquad \text{(IV)}$$

$$\text{for } V \leqslant Vc,$$

$$Ni(V) = C'T^2[6k^2T^2 + 4kT(V - Vc) + (V - Vc)^2]\cdot\exp[-\phi/kT]$$

$$\text{for } V \geqslant Vc. \qquad \text{(V)}$$

If Ni(V) is now plotted as a function of V, these equations will yield a theoretical ionization efficiency curve which, according to Honig(9), approaches an exponential line below the appearance potential.

However, there are other phenomena affecting the electron beam that are not as conveniently treated. Energy spreads may be caused

by the potential drop along the filament, the filament temperature (and therefore the filament current), and most important of all, the various ion-repeller fields in the ionization chamber. These effects can generally be accounted for by injecting a calibrating gas, whose appearance potential is accurately known, along with the sample. The ionization efficiency curves are then determined simultaneously and the appearance potential of the calibrating gas is adjusted to its correct value. Then by adjusting the unknown by the same amount, an accurate determination of the appearance potential can be made using procedures to be discussed later.

B. THE APPLICATION OF APPEARANCE POTENTIALS

It is apparent that appearance potentials and ionization potentials are closely related. For the electron-impact process

$$A + e = A^+ + 2e \qquad \text{(VIII)}$$

it follows that

$$A.P.(A^+) = I.P.(A) + KE + EE$$

where $A.P.(A^+)$ is the appearance potential of A^+, $I.P.(A)$ is the adiabatic or spectroscopic ionization potential, KE is the excess kinetic energy, and EE is the excitation energy (rotational, vibrational, and electronic). It readily follows from the definitions in section I-C that I.P.(adiabatic) = I.P.(vertical) - EE.

For the situation where A^+, a parent ion, is formed without any excess energy, then A.P. = I.P. This is the case for Franck-Condon transitions as shown in figure 3-A, the electronic potential curves of the ground state of the molecule and of the ground state of the ion

being in alignment. The appearance potential of a parent ion, therefore, at worst will give an upper limit to the ionization potential; hence, some information is gained as to the energy of the highest occupied molecular orbital. Usually the terms "ionization potential" and "appearance potential" are used synonymously as applied to parent ions.

The inert gases are an example of the simple process shown in reaction (VIII). As the spectroscopic (adiabatic) ionization potentials are known to a high degree of precision for these elements, they are almost always used as calibrating gases in the mass spectrometer.

Appearance potentials are also useful in determining dissociation energies and heats of formation. The reaction between an electron and a molecule AB can be written

$$AB + e = A + B^+ + 2e. \qquad (IX)$$

Therefore, the relation between the appearance potential $A.P.(B^+)$ and the ionization potential $I.P.(B^+)$ is (neglecting KE and EE):

$$A.P.(B^+) = I.P.(B^+) + D(AB)$$

where D(AB) is the dissociation energy of AB. This can be determined if the ionization potential is known and if KE = EE = 0. Once the dissociation energy is known, other thermodynamic quantities may be calculated. For example, the chemical dissociation AB = A + B has an enthalpy of reaction that equals the dissociation energy:

$$D(AB) = \Delta H_f(B) + \Delta H_f(A) - \Delta H_f(AB). \qquad (X)$$

Accordingly, heats of formation may be calculated if sufficient enthalpy data is available.

Similarly, by recognizing that the appearance potential of

B^+ is numerically equal to the heat of reaction in (IX), it follows that

$$A.P.(B^+) = \Delta H_f(B^+) + \Delta H_f(A) - \Delta H_f(AB). \qquad (XI)$$

Therefore, the ionic heat of formation, $\Delta H_f(B^+)$, can be determined.

In the above cases, the problem of the initial kinetic energy has been avoided by assuming it to be zero. A useful empirical observation for saturated hydrocarbons in this regard is Stevenson's Rule:(11) For a molecule AB where I.P.(A) is greater than I.P.(B), there are two possible processes of dissociation, namely

$$AB + e = A + B^+ \qquad (XII)$$

and

$$AB + e = A^+ + B. \qquad (XIII)$$

Stevenson has observed that equation (XII) occurs such that A and B^+ are formed in their ground states with no additional energy, while for reaction (XIII), A^+ will usually be formed with excess energy.

McDowell and Warren(12) have shown that if an ion is formed with appreciable kinetic energy there will be some effect on the distribution of the intensity of the focussed ionic beams reaching the collector slit. Therefore, if there is an increase in the width of the m/e intensity peak with a change in the ion accelerating potential, a slight defocusing is indicated due to the initial energy.

Fortunately, however, many ions formed in electron-impact induced dissociations have very nearly zero excess kinetic energy(13). Morrison and Stanton(14) have claimed, moreover, that fragment ions with excess energy give rise to an error of only 0.05 e.v. in the appearance potential - well within the error that is normally associated with fragment ions. Although it is difficult to draw conclusions from appearance

potentials of fragment ions, ionization potentials of parent ions can often be determined quite accurately. How this is done will be considered in the next section.

C. THE DETERMINATION OF APPEARANCE POTENTIALS

H. D. Smyth[15] was the first to employ a low energy electron-impact apparatus coupled with a positive ion mass analyser to measure ionization efficiency curves. Taking the ionization potential to be where the ion current just disappeared, his values for Hg^{++} varied from 4 to 5 volts in experimental deviation. Since this time, the development that has taken place in instrumentation and experimental techniques enables ionization potentials to be determined to a few hundredths of a volt in mean deviation. Nevertheless, it appears that determinations by different workers can vary by as much as 0.5 volts[16] - presumably, the value depending on the type of mass spectrometer used. When obtaining values for ionization potentials, therefore, as determined by electron-impact, it is desirable that values from several different sources be considered and the most consistant values used.

The basic problem in interpreting ionization efficiency curves is the initial curvature at low electron energies. This renders the actual location of the "disappearance" of the ionic current somewhat doubtful. Accordingly, various methods have been proposed to overcome this problem, all of them involving the use of a calibrating gas whose curve is determined simultaneously with the unknown. For the most accurate results, Mitchel and Coleman[17] have shown that a calibrant should be chosen whose ionization potential does not differ significantly from the appearance potential of the ion being determined. As was pointed

out previously, the internal calibrant overcomes the errors due to the effect of the various magnetic and electric fields existing in the ion source. Obviously, these effects will be greatest at the low electron energies - that is, in the region where the most precise measurements are required.

It would seem evident that the most desirable technique would be to eliminate that part of the initial curvature or "foot" in the ionization efficiency curve caused by the spread in electron energy. Fox[10,18,19,] has done this by constructing a retarding potential difference source which repells the low-energy electrons emitted from the filament. Recently, Marmet and Kerwin (20) have used an energy filter system that produces an energy spread of less than 0.1 e.v.

Once the energy spread has been eliminated, it is possible to locate breaks in the curves corresponding to electronic transitions to excited vibrational levels in the ion. Morrison[7], making the assumption that the separate values of the probabilities for transitions to all possible states are additive, has observed that the presence of each of these processes is shown by peaks in the second derivative of the ionization efficiency curve. Hence, Marmet and Kerwin[20] were able to resolve the fine structure in argon and to measure vibrational levels in N_2^+, NO^+, and H_2^+. However, few mass spectrometers are equiped with such sophisticated equipment and more approximate methods must be used.

Generally speaking, the common methods that have been developed to obtain appearance potentials from ionization efficiency curves may be summarized under two main headings: (1) the Linear Extrapolation

(L.E.) procedure, and (2) the Vanishing Current (V.C.) procedure. The first of these, the Linear Extrapolation method, is undoubtably the most direct technique and is the easiest to apply experimentally. The linear portions of the ionization efficiency curves for both the standard and the unknown are simply extrapolated back to zero ion current (see figure 6-A). Then by adjusting the energy scale so that the linear intersect of the standard intersects the energy scale at its spectroscopic value, the intersect of the 'unknown' ion yields the appearance potential. It is argued that the values obtained in this way correspond closely to the energy necessary to produce transitions through the centre of the Franck-Condon region[21]. However, in nearly all cases the ionization potential determined by this method is larger than the actual value as obtained by spectroscopy[22], suggesting that the L.E. procedure is only useful for placing an upper limit on the possible values. Consequently, despite its relative simplicity, the L.E. method is no longer used.

Instead of disregarding the "foot" of the curve as in the above case, the Vanishing Current method attempts to determine the actual point on the initial curvature corresponding to the onset of ionization. Compared to the L.E. procedure, the V.C. methods usually give lower results for ionization potentials which are in greater accord with spectroscopic values[23].

The original V.C. technique, as proposed by P. T. Smith[24], which he used to study the rare gases He,Ne, and Ar, employed an "initial upward break" procedure. Smith attempted visually to find the point on the ionization efficiency curve where the "initial break"

FIGURE SIX

THE DETERMINATION OF APPEARANCE POTENTIALS

A VOUGHT LINEAR EXTRAPOLATION METHOD
B SMITH INITIAL BREAK METHOD
C,D WARREN EXTRAPOLATED VOLTAGE DIFFERENCE METHOD

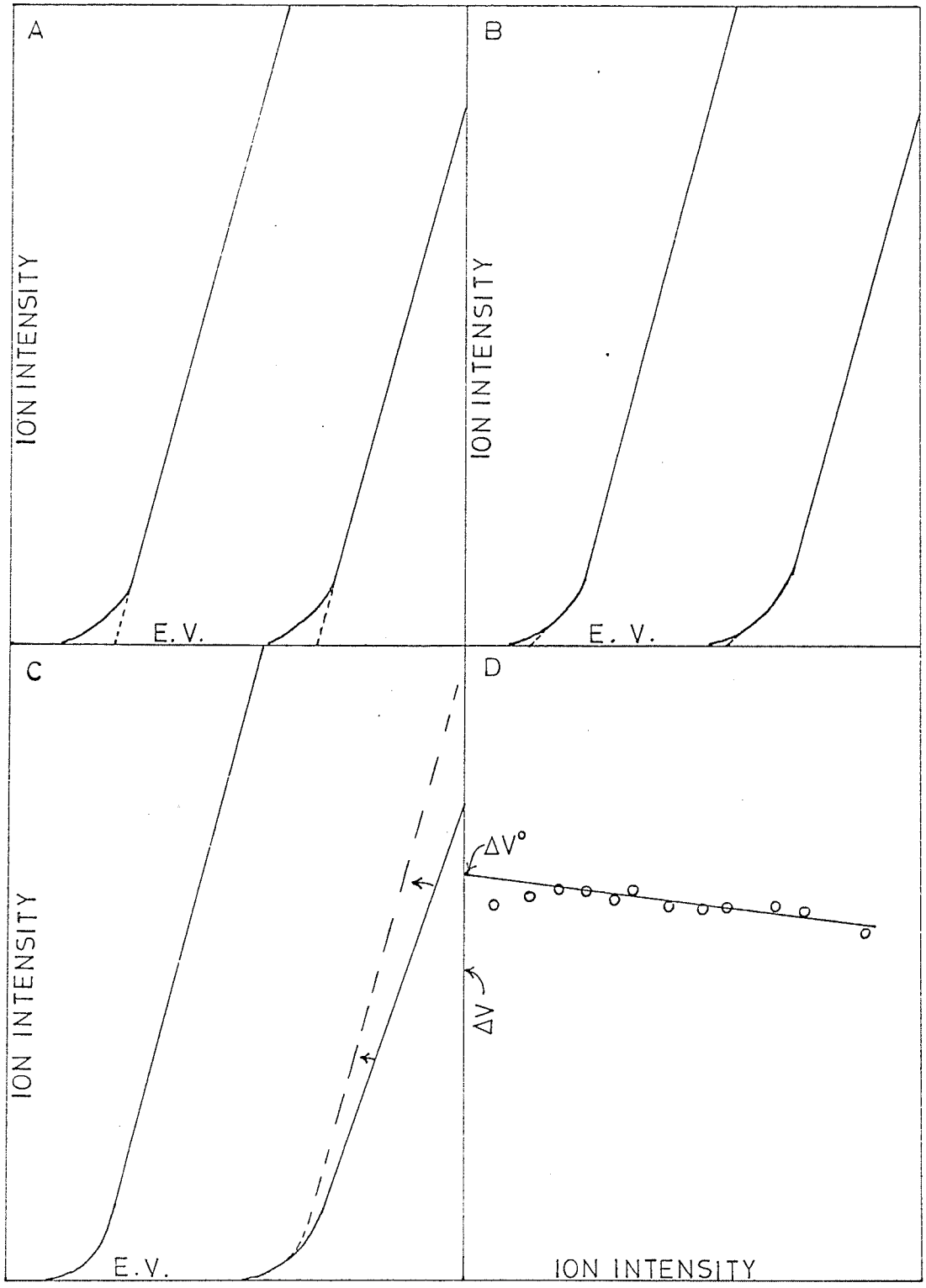
A
ION INTENSITY
E.V.
B
ION INTENSITY
E. V.
C
ION INTENSITY
E.V.
D
ΔV°
ΔV
ION INTENSITY

occurs - that is, the point on the curve where the "foot" begins to obscure the primary ionization. Once this point is found, the curve is extrapolated to zero ion current, the justification being that the curve would follow this path were it not for the electron energy spread (see figure 6-B). However, as the plot tends to approach the energy axis almost assymptotically, there is rarely a sharp break that can be observed with some degree of objectivity. In most cases, therefore, the actual assigning of the initial break in the curve becomes somewhat arbitrary[25]. Nevertheless, Mariner and Bleakney[26] have been able to locate breaks in the ionization efficiency curve to 0.05 of a volt under conditions of high sensitivity. Stevenson and Hipple[27] used the V.C. "initial break" procedure to determine the difference between the ionization potentials of Ne and Ar. Their value of 5.65 ± .15 e.v. compares favourably with the spectroscopic value of 5.80, within the .15 e.v. error. It has been found, however, that the ionization potential determined in this way will depend on several external variables (e.g. sample pressure, electron current, amplifier sensitivity)which have nothing to do with the inherent nature of the sample[4]. It must be concluded, therefore, that the "initial break" procedure ought not to be applied where accurate determinations are necessary.

J. W. Warren[28] has proposed an "extrapolated voltage difference" technique for finding the point of vanishing current which is more satisfactory than Smith's method. Once the ionization efficiency curves of the standard and the unknown have been obtained, the ion current scale of either the calibrant or the sample is arbitrarily adjusted to make the linear portions of the curves parallel. The voltage differences

between the two curves, ΔV, are determined for various values of I, the ion current. Then by plotting ΔV against I and extrapolating the resulting linear curve to zero ion current, ΔV^o, the energy difference at zero ion intensity is obtained. ΔV^o is considered to correspond to the difference between the ionization potentials of the sample and the calibrant (see figures 6-C and 6-D). Although the adjusting of the ionization efficiency curves is difficult to justify theoretically, the values obtained are reasonably close to spectroscopic values[28]. However, it has been found that the "extrapolated voltage difference" method is not suitable for measuring the appearance potentials of ions formed with very low intensities[29].

A method with reasonably sound theoretical basis is the "critical slope" procedure developed by Honig[9]. Taking the logarithm of Ni(V) in equation IV and plotting the resulting expression against the electron acceleration voltage, V, then in the region of the "critical voltage", Vc, the slope of the semilogarithmic curve will be

$$\frac{d}{dV}\left[\log Ni(V)\right] = 1/kT - \left[1/(Vc - V + 3kT)\right].$$

At the critical energy where V = Vc, the slope is therefore

$$\frac{d}{dV}\left[\log Ni(V)\right]_{critical} = 2/3kT.$$

Consequently, by applying a tangent of critical slope 2/3kT to the semilogarithmic ionization efficiency plot, the point of contact on the curve yields the appearance potential. (see figure 7-A)

Honig's idea of using a semilogarithmic plot has been utilized in a simple modification by Lossing, Tickner, and Bryce[30]. Their empirical approach is based on the initial (low energy) shapes of the

FIGURE SEVEN

THE DETERMINATION OF APPEARANCE POTENTIALS

A HONIG CRITICAL SLOPE METHOD
B LOSSING, TICKNER, BRYCE METHOD
C MAXWELLIAN ELECTRON THERMAL ENERGY SPREAD REDUCTION USING WINTER'S METHOD
D COMPARISON OF THE $\Delta N_i(V)$ FUNCTION WITH THE PROBABILITY OF IONIZATION $p(E)$ AND THE NORMAL IONIZATION EFFICIENCY CURVE $N_i(V)$

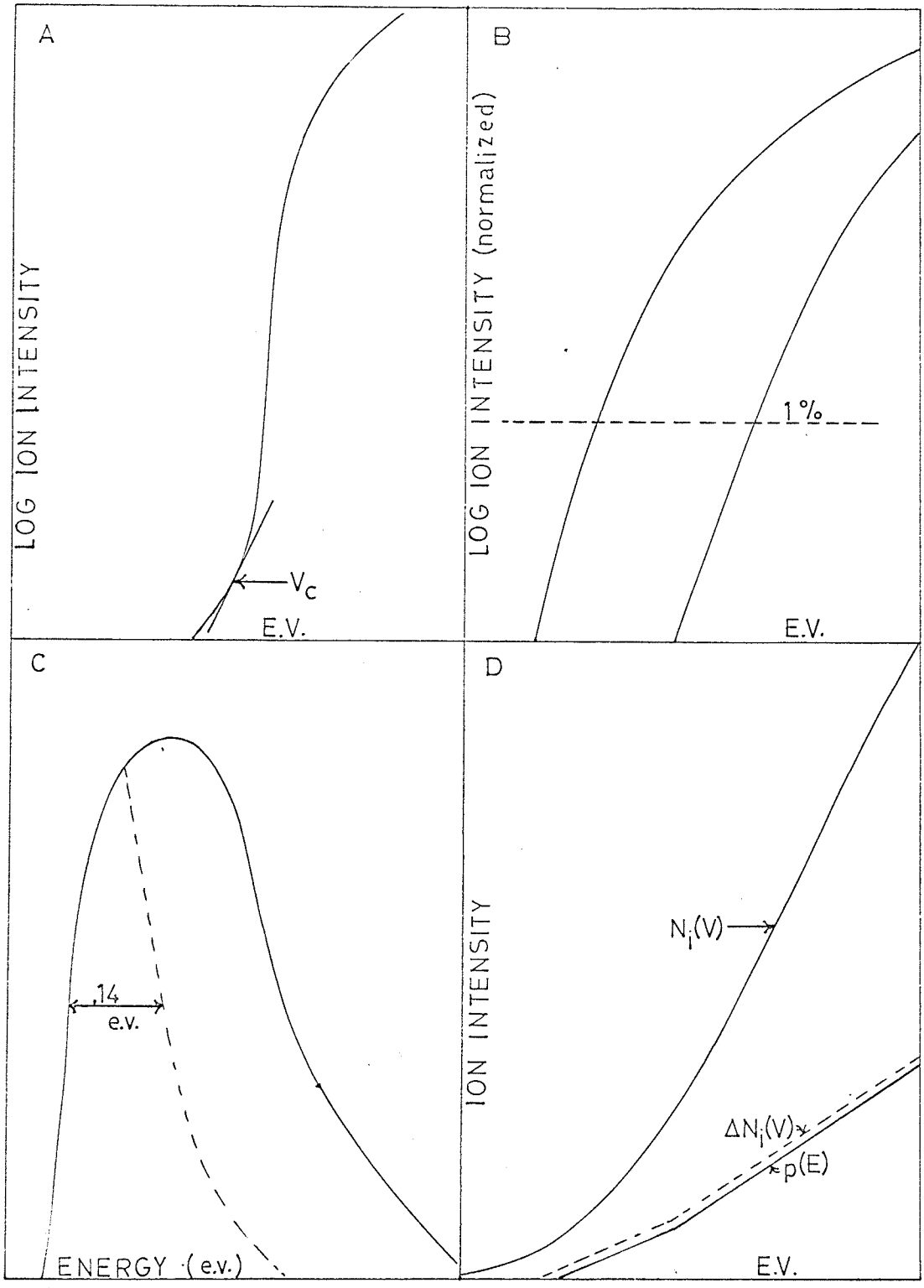
A
LOG ION INTENSITY
V_c
E.V.
B
LOG ION INTENSITY (normalized)
1%
E.V.
C
.14
e.v.
ENERGY (e.v.)
D
ION INTENSITY
$N_i(V)$
$\Delta N_i(V) \times p(E)$
E.V.

ionization efficiency curves for a large number of compounds. It was found that if the sample pressures of the standard and the unknown were adjusted to give the same ion peak height at an electron energy of 50 e.v., then the ionization efficiency curves were exponentially parallel in the region where the ion intensities are approximately one percent of their values at 50 e.v. Therefore, by normalizing the semi-logarithmic curves of the standard and unknown to a 100% value at 50 e.v., the energy difference at 1% peak height is taken as the difference in the ionization potentials of the calibrant and the unknown (see figure 7-B).

Lossing, Tickner and Bryce[30] also use a simplified procedure to obtain an estimate of the ionization potential that does not necessitate the determination of the whole ionization efficiency curve. Once it has been ascertained that the curves for the standard and unknown are parallel in the one percent ion current region, it is simply necessary to adjust the ion intensities (by varying the respective sample pressures) to the same value at 50 e.v. and to measure the electron energy difference when the intensities of the two ions are at their respective one percent values. Therefore, an appearance or ionization potential can be determined in a matter of minutes. It is claimed that a reproducibility of $\pm$0.01 e.v. is possible utilizing this procedure. A slight modification of the method is used by Dibeler and Reese[31] who normalize the ion intensities to a 100% value at 70 e.v.

Recently, R. E. Winters[32] has developed an "energy distribution difference" method which involves a simple mathematical transformation of the normal ionization efficiency curve data. Equation II

gave the ion current as

$$Ni(V) = \int Ne(U)p(E)dE.$$

At some other electron acceleration voltage V', the expression becomes

$$Ni(V') = \int Ne(U')p(E)dE.$$

If this equation is multiplied by a constant b and subtracted from the equation for Ni(V), then

$$\begin{aligned} \Delta Ni(V) &= Ni(V) - bNi(V') \\ &= \int [Ne(U) - bNe(U')]p(E)dE. \end{aligned}$$

The difference term in brackets is a new energy distribution in the electron current, ΔNe. Hence, the expression can be written

$$\Delta Ni(V) = \int \Delta Ne\ p(E)dE.$$

The new energy function, ΔNe, has a Maxwellian distribution (see figure 7-C) which effectively reduces the spread in electron energy to 0.14 e.v.[32]

The physical significance of $\Delta Ni(V)$ is that it is the difference in ion current between ionization produced by N electrons at a voltage V and ionization produced by bN electrons at a slightly higher voltage V'. The best set of parameters b and ΔV (= V - V') can be obtained from the experimental data by choosing them such that the exponential portions of the Ni(V) and bNi(V') curves coincide. When this is the situation, $\Delta Ni(V)$ is almost zero in this region and the effect of the energy spread in Ne(U) is eliminated. The expression $\Delta Ni(V) = Ni(V) - bNi(V')$ produces an ionization efficiency curve which is almost identical to p(E), the probability of ionization (see figure 7-D).

In conclusion, any of the common empirical methods discussed above would give the correct results if all ionization efficiency curves

had the same shape and were parallel. As it is, comparative studies show that the methods are usually reproducible to $\pm$0.1 e.v.[33] of the spectroscopic values when these are available. The problem of evaluating the appearance potential is mainly one of interpreting the ionization efficiency curve, which in the case of fragment ions is no mean task due to the large number of processes which could be taking place. In short, then, ionization potentials of parent ions can often be determined quite accurately, while appearance potentials of fragment ions should be treated with some degree of caution.

APPARATUS AND PROCEDURE

FIGURE EIGHT

THE HITACHI-PERKIN-ELMER RMU 6-D
MASS SPECTROMETER COUPLED WITH
THE HONEYWELL 1608 VISICORDER

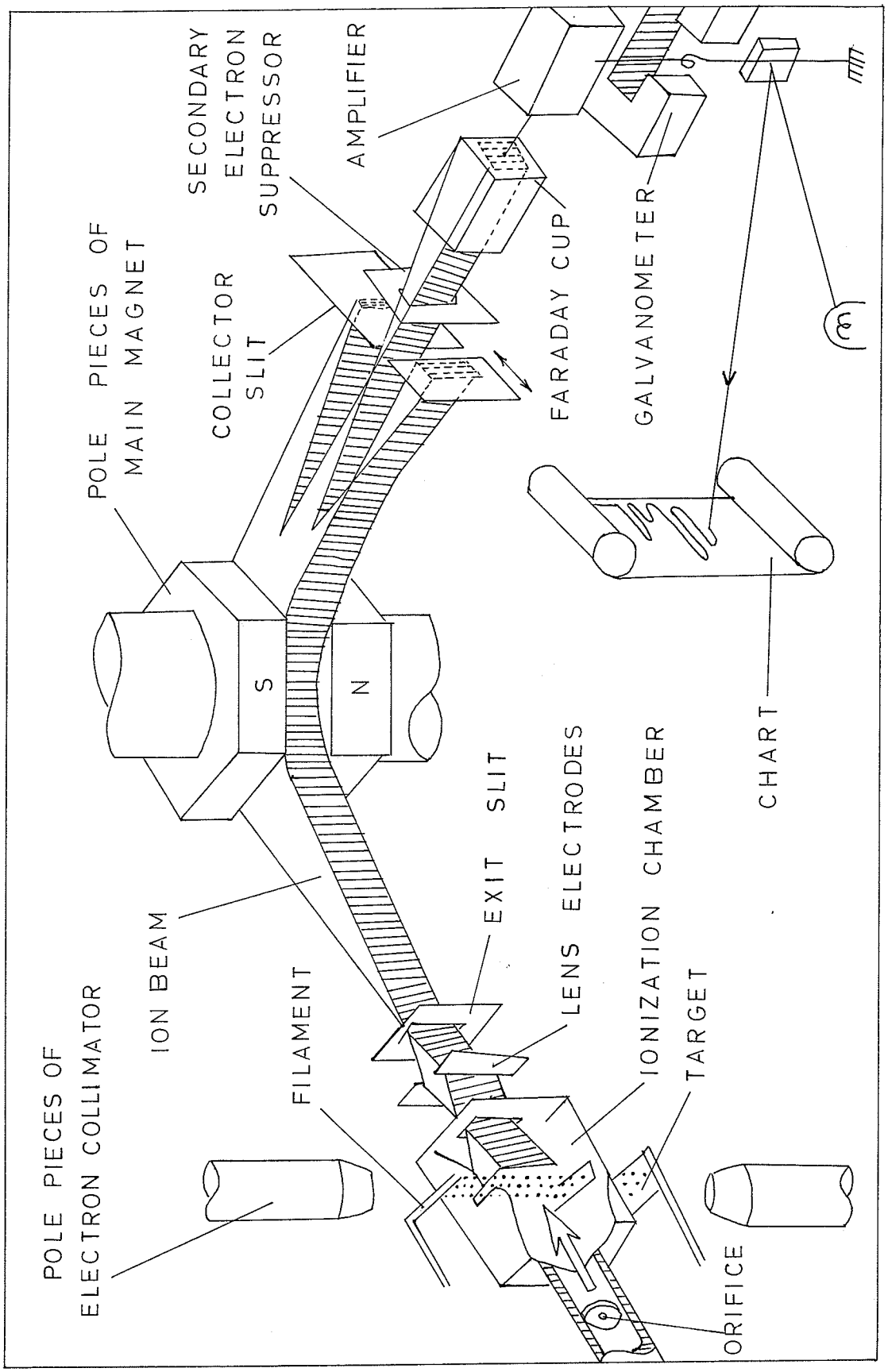
POLE PIECES OF ELECTRON COLLIMATOR
ION BEAM
FILAMENT
POLE PIECES OF MAIN MAGNET
S
N
COLLECTOR SLIT
SECONDARY ELECTRON SUPPRESSOR
AMPLIFIER
FARADAY CUP
GALVANOMETER
EXIT SLIT
LENS ELECTRODES
IONIZATION CHAMBER
TARGET
ORIFICE
CHART

system crossing an ion optical system. The basic technical problem in any ion source is how to maintain the electron-matter interaction at a maximum while maintaining the interaction of the two optical systems at a minimum.

As shown in figure 8, the sample has passed through an orifice, is ionized by the electron beam, and is accelerated and focused by a set of electrodes situated in front of the ion chamber. Figure 9 illustrates the various components of the T-2M ion source. The electrons are emitted from a hot filament, accelerated through the ion chamber by a potential applied between the filament and the chamber wall (the "chamber voltage"), and strike a target maintained at a positive potential with respect to the chamber wall. The divergence of the electron beam is made as small as possible by use of a collimating magnet (figure 8), and by a grid electrode located behind the filament (figure 9) which can be varied between 0 and -20 volts with respect to the filament. On the edge of the "pull slit" in figure 9 are located two iron pole pieces which serve to concentrate the flux of the external collimator magnet.

The grid, chamber, and target voltages can all be varied by means of potentiometers located on the ion source panel. The chamber voltage, which constitutes the electron acceleration potential, can be varied from about 2 to 100 volts with respect to the filament, while the target voltage is usually maintained 40 to 50 volts above the chamber.

The electron emission from the filament, which is stabilized when the current through the filament is about 3 amperes for Re wire

FIGURE NINE

THE T-2M ION SOURCE

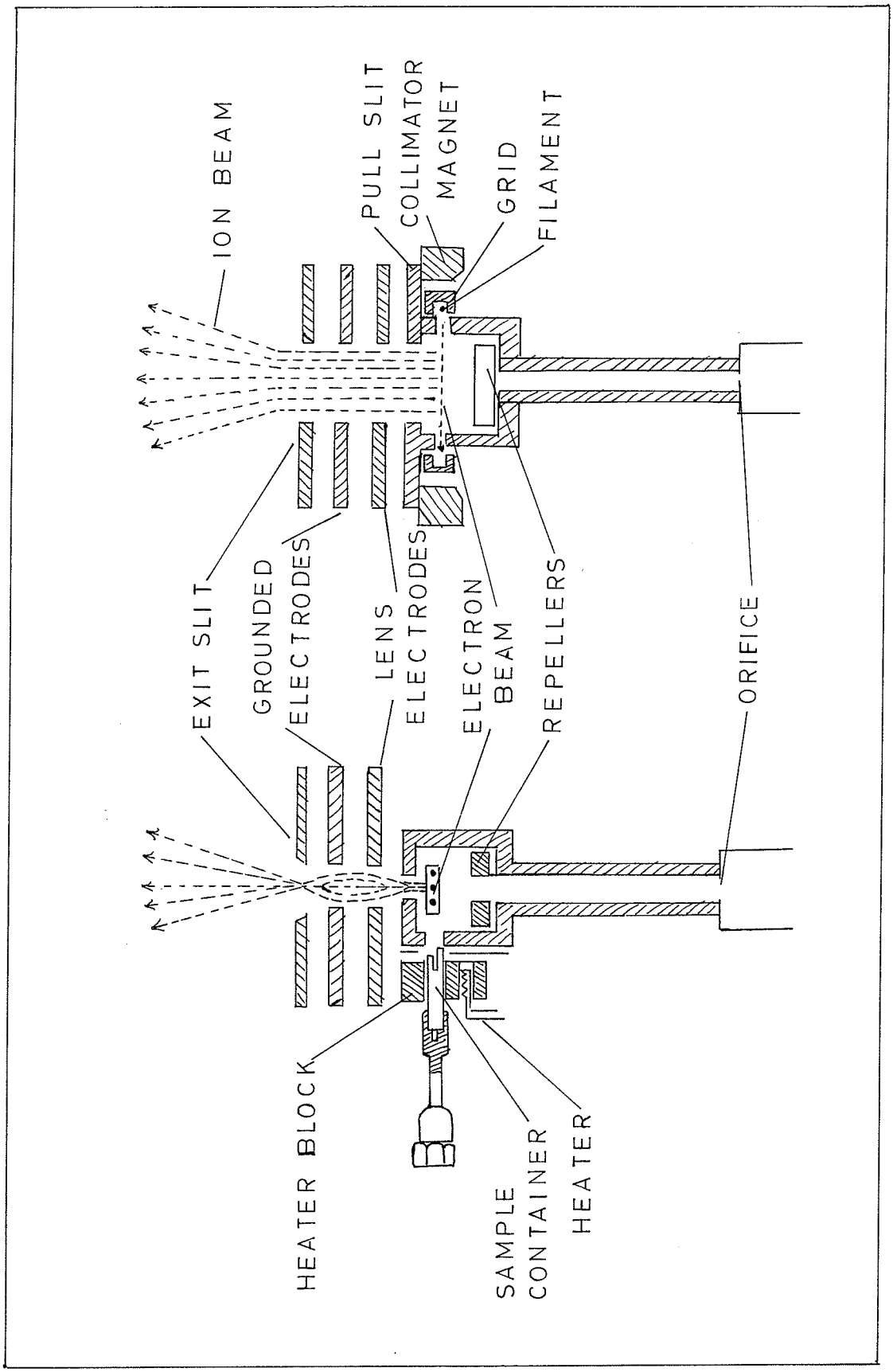
ION BEAM
PULL SLIT
COLLIMATOR MAGNET
GRID
FILAMENT
EXIT SLIT
GROUNDED ELECTRODES
LENS ELECTRODES
ELECTRON BEAM
REPELLERS
ORIFICE
HEATER BLOCK
SAMPLE CONTAINER
HEATER

of .18 mm diameter, has a maximum value of 200 micro-amperes, although it is normally set at a value below 100 micro-amperes to preserve the filament. The current reaching the target should be 50 to 90 percent of the emission and can be improved by adjusting the collimating magnet. Both the filament and target are mounted on glass assemblies to effect their easy removal, the target assembly also including coils to heat the ionization chamber (250°C). This is to prevent contamination of the ion source as well as any thermal deviations in pattern coefficients. The heater coils are well removed from the filament to prevent any thermal distortion.

Once the ions have been formed by the electron beam, they are "pushed" into the ion accelerating field by a potential gradient between two repeller electrodes (see figure 9). A maximum D.C. potential of 3600 volts is impressed between the "pull slit" and the grounded electrodes which serves to accelerate the ions into the magnetic analyser field. Located between these plates are a pair of lens electrodes which focus the ion beam in the vicinity of the grounded exit slit. By adjusting the potential on the repeller and lens electrodes, the ionic current reaching the collector can be maximized.

(b) Magnetic Analyser

Once the ions leave the ion source, they are acted upon by a perpendicular magnetic field which curves the ion beam through a 90°, 8 inch radius sector. As the spectrum is scanned, the current through the coils of the electromagnet producing the field increases to 300 milliamperes, at which point the field strength becomes 8,000 to 9,000 gauss.

If the background spectrum in the mass spectrometer becomes large, it is required that the analyser tube be baked. This is accomplished by passing current (100 amperes) directly through the tube at a low voltage (1 volt). The only other maintenance necessary is to reverse the magnetic coil current from time to time to prevent the permanent magnetization of the magnet's core.

(c) Detector System

The ion beam may be detected either by a Faraday cup or by an electron multiplier, which can easily be interchanged externally. The advantage of the Faraday cup is its relative stability, while the electron multiplier is used for its greater sensitivity. In determining ionization efficiency curves, the electron multiplier is almost always used in order that small ion intensities at low electron bombarding energies can be detected.

Once the signal has been amplified, it enters the Honeywell 1608 Visicorder. The Visicorder is a 4-channel galvanometric recorder with a linearity of $\pm 2\%$. Ultraviolet light falling on the face of a galvanometer is reflected by a small mirror attached to its torsion wire onto U.V. sensitive paper which almost instantly reproduces the trace. The sensitivities of the galvanometers are approximately in the ratio 27/9/3/1, thus insuring a wide range of ion intensities can be reproduced on the graph paper.

PART TWO: EXPERIMENTAL CONSIDERATIONS

The measurement of ionization efficiency curves involves the careful consideration of the various inter-related settings on the mass spectrometer. The chamber voltage, target voltage, grid voltage, total emission current from the filament, and filament current can all be adjusted by means of potentiometers as indicated in figure 10. The chamber potentiometer is doubly-ganged, R4 controlling the voltage on the chamber wall, while R1 insures that the potential difference between the target and the chamber remains constant when the chamber voltage is varied. The target voltage can also be independently varied by adjusting R2. The grid potentiometer, R3, controls the negative potential on the grid with repect to the filament. The total emission current and filament current potentiometers, R5 and R6 respectively, control the output stages from an emission stabilizer circuit.

Often it becomes necessary to compromise between the optimum conditions of two variables in order to obtain the greatest accuracy. For example, figure 11 indicates the linear dependence of the ion intensity for He^+ on the total electron emission from the filament. Ostensibly, it would seem desirable to choose the largest emission possible in order to obtain the greatest sensitivity. The choice of an emission current is somewhat complicated, however, by the fact that it must remain constant throughout the entire measurement - otherwise, there will be no correlation between intensity measurements. It has also been suggested that the electron emission be kept as low as possible[19,31] due to the fact that an increase causes the linear portion of the ionization

FIGURE TEN

DIAGRAM OF THE CHAMBER VOLTAGE, TARGET VOLTAGE, GRID VOLTAGE, TOTAL EMISSION CURRENT, AND FILAMENT CURRENT POTENTIOMETERS AND THEIR CONNECTIONS TO THE ELECTRODES IN THE ION SOURCE

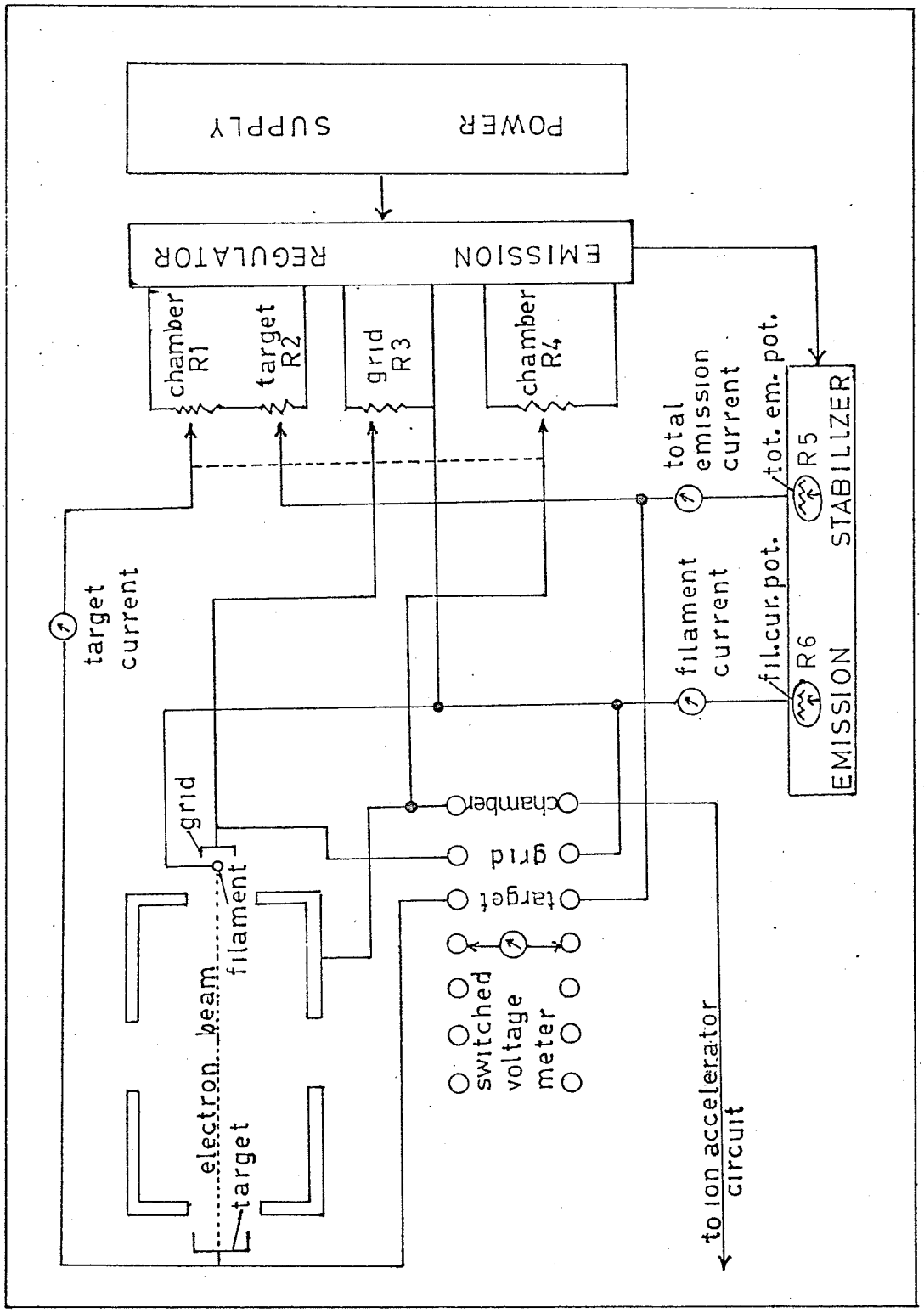
POWER SUPPLY
EMISSION REGULATOR
chamber R1
target R2
grid R3
chamber R4
total emission current
tot. em. pot.
R5
STABILLZER
EMISSION
R6
fil.cur.pot.
filament current
target current
grid
chamber
grid
target
switched voltage meter
filament
electron beam
target
to ion accelerator circuit

FIGURE ELEVEN

RELATION BETWEEN THE TOTAL ELECTRON EMISSION AND THE ION INTENSITY FOR He^+ (M/E 4)

CONDITIONS:

Target Voltage: 40 volts above chamber
Chamber Voltage: 50 volts
Grid Voltage: -10 volts
Ion Acceleration Voltage: 1800 volts

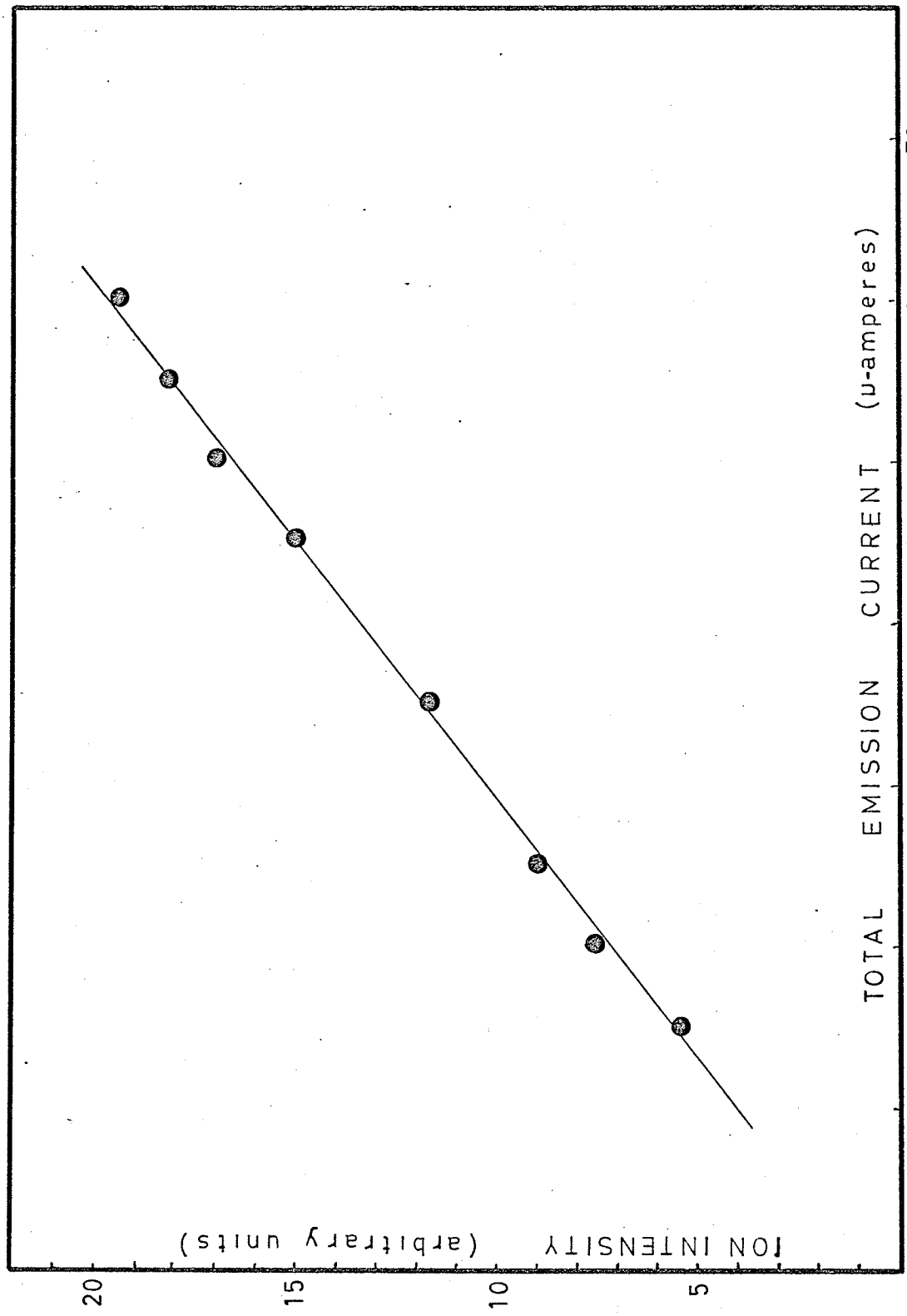
ION INTENSITY (arbitrary units)
TOTAL EMISSION CURRENT (μ-amperes)
0
10
20
30
40
50
60
70
5
10
15
20

efficiency curve to slip along the energy axis and the "foot" of the curve increases.

It has been found that a set value of the emission current can be maintained constant at low chamber voltages by choosing an appropriate value for the grid potential. Figure 12 shows how the emission and filament currents vary with the grid voltage when the chamber potential is in the region where appearance potentials normally occur (10 volts). The emission (open circles) was initially set at 50 microamperes for a grid potential of -1 volt. As the grid voltage is increased (made more negative), the emission remains constant until the grid becomes -8 volts, at which point there is a rapid decline. The filament current, on the other hand, begins to rise when the grid is at -2 volts. This increase offsets the tendency for the emission to fall as the grid becomes more negative. However, as the filament current begins to level off to a maximum, no further stabilization of the emission is possible. It is obvious, therefore, that a grid setting above-8 volts is not acceptable for measuring ionization efficiency curves. The only adverse result of rendering the grid potential more positive is the effect on the intensity of the ionizing electron beam. This, however, cannot be avoided.

It is desirable, then, to choose the grid voltage such that the emission will remain constant when the chamber potentiometer, which controls the electron energy, is varied over a wide range. Figure 13 illustrates how the electron energy varies with the chamber potentiometer when the grid is maintained at -2 volts, the emission being 20 microamperes. As the chamber potentiometer is changed in the direction of

FIGURE TWELVE

THE DEPENDENCE OF THE TOTAL
ELECTRON EMISSION AND FILAMENT
CURRENT ON THE GRID POTENTIAL

● ....FILAMENT CURRENT
○ ....EMISSION CURRENT

CONDITIONS:

Chamber Voltage: 10 volts
Target Voltage: 44 volts above chamber
Ion Acceleration Potential: 3600 volts

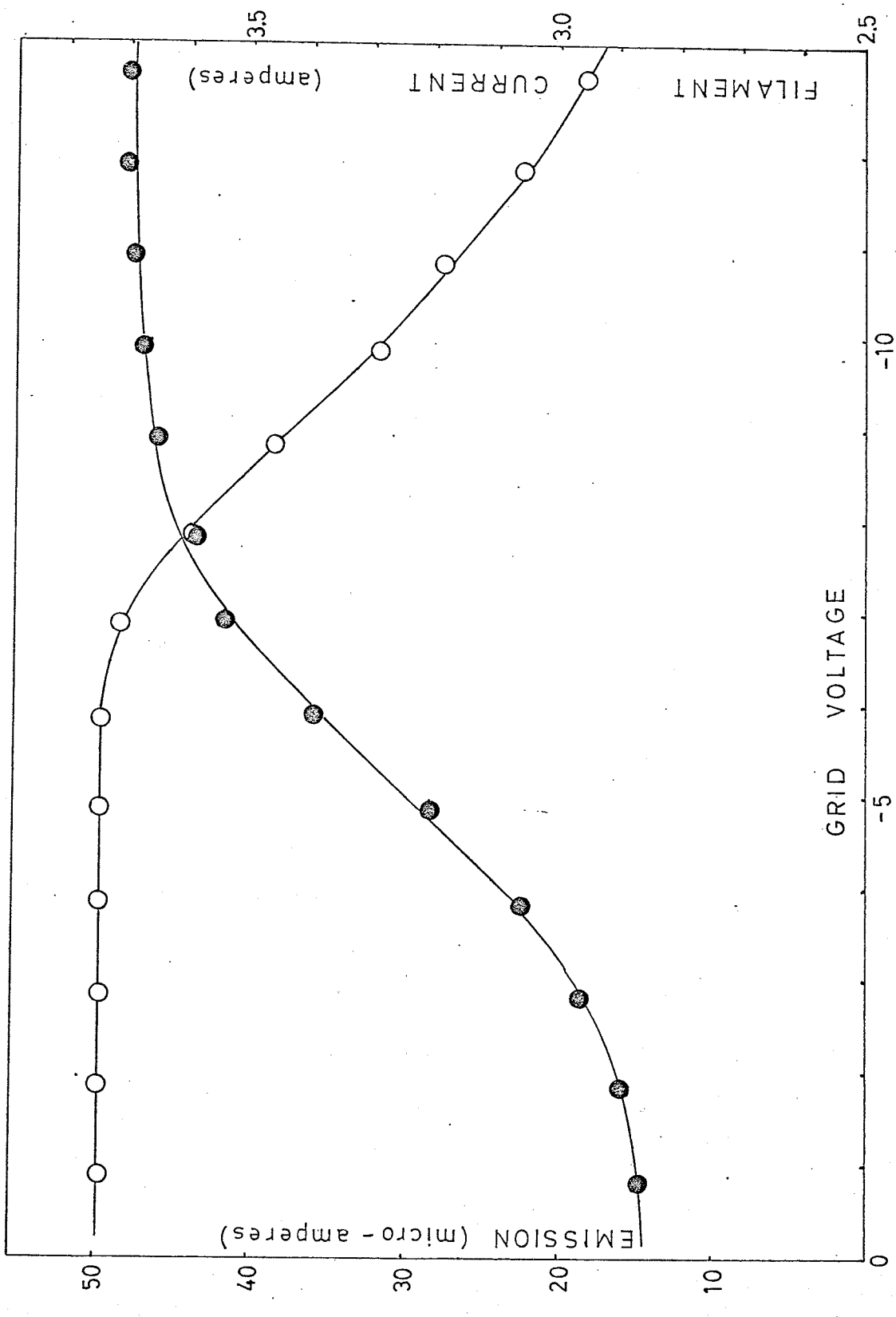
EMISSION (micro - amperes)
50
40
30
20
10
0
-5
-10
GRID VOLTAGE
2.5
3.0
3.5
FILAMENT CURRENT (amperes)

FIGURE THIRTEEN

RELATIONSHIP BETWEEN THE CHAMBER POTENTIOMETER READING AND THE ELECTRON ENERGY

(AS MEASURED ON AN EXTERNAL POTENTIOMETRIC CIRCUIT)

CONDITIONS:

Total Emission Current: 20 micro-amperes
Target Current: approx. 10% of the emission
Ion Acceleration Potential: 1800 volts
Target Voltage: 40 volts above chamber
Grid Voltage: -2 volts

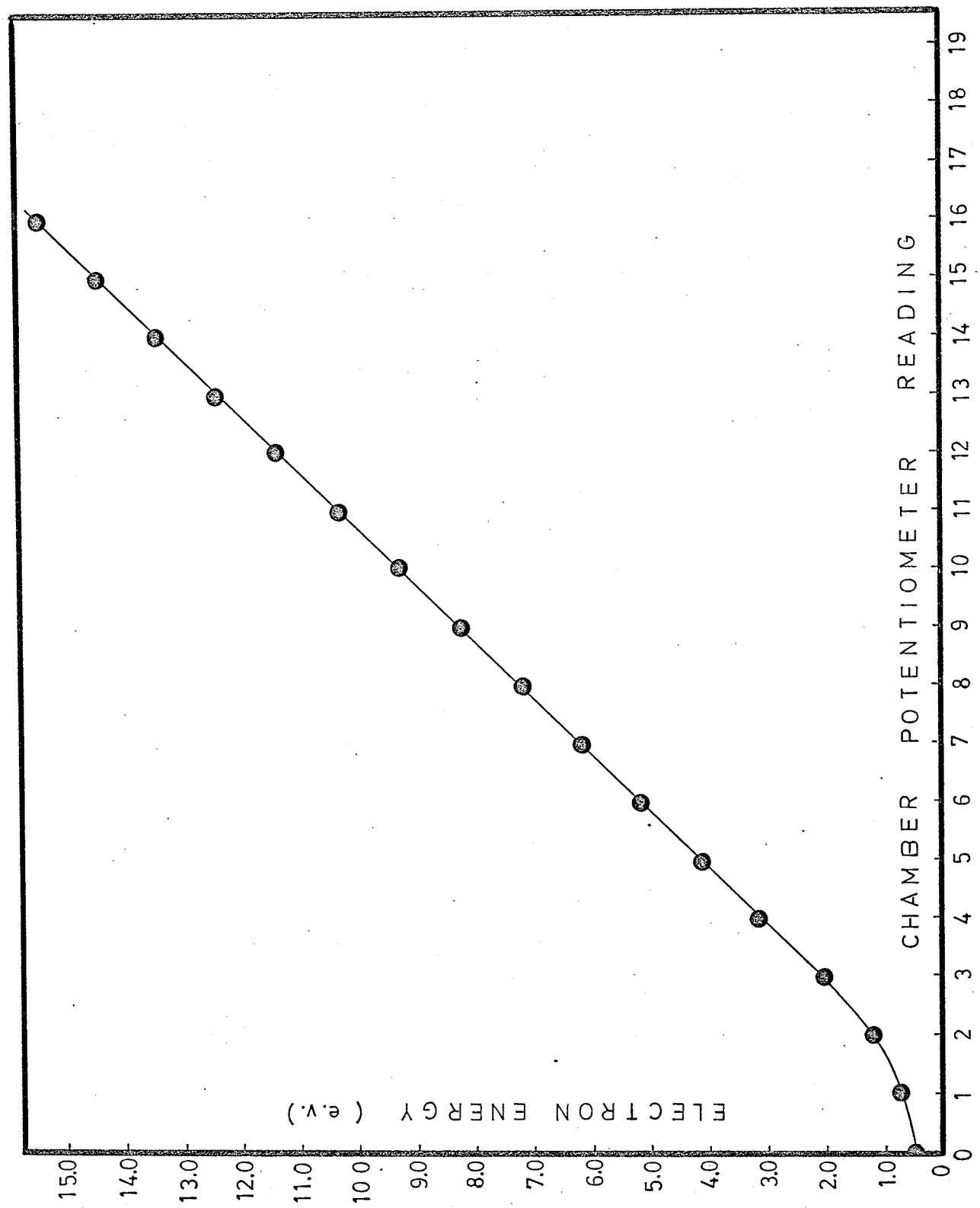
ELECTRON ENERGY (e.v.)
15.0
14.0
13.0
12.0
11.0
10.0
9.0
8.0
7.0
6.0
5.0
4.0
3.0
2.0
1.0
0
CHAMBER POTENTIOMETER READING
0 1 2 3 4 5 6 7 8 9 10 11 12 13 14 15 16 17 18 19

decreasing electron energy, the energy change is linear until about 2 e.v. These readings may now be applied to figure 14 which indicates how the total emission current varies with the chamber potentiometer reading when the grid is -2 volts. The emission current was stabilized at 20 micro-amperes at a chamber potentiometer reading of 40, and the emission was recorded as the chamber potentiometer was changed in the direction of decreasing electron energy. As indicated, the emission remains constant until the chamber potentiometer dial is at 3, which from figure 13, corresponds to an electron acceleration potential of 2 volts - that is, well below the appearance potential of most ions. Consequently, a grid setting of -2 volts appears to be quite adequate for determining ionization efficiency curves.

Figure 14 showed that the electron energy varies linearly with the chamber potentiometer setting for a fixed value of the emission current and grid voltage. However, the electron energy does not stay constant if either the emission or grid potentiometer is changed when the chamber potentiometer is in a fixed position. Figure 15 shows how the electron energy changes with the total emission current when the chamber potentiometer is in a fixed position corresponding to 10 volts (as measured on an external potentiometric circuit) at a total emission of 50 micro-amperes and a grid setting of -2 volts. Stabilization was attained by increasing the current through the filament just up to the point where the emission current and filament current became constant. Above 50 micro-amperes, the electron energy increases, while below this

FIGURE FOURTEEN

RELATIONSHIP BETWEEN THE TOTAL
EMISSION CURRENT AND THE CHAMBER
POTENTIOMETER DIAL READING

CONDITIONS:

Target voltage: 44 volts above chamber
Target current: approx. 20% of emission
Grid voltage: -2 volts
Ion acceleration voltage: 1800 volts

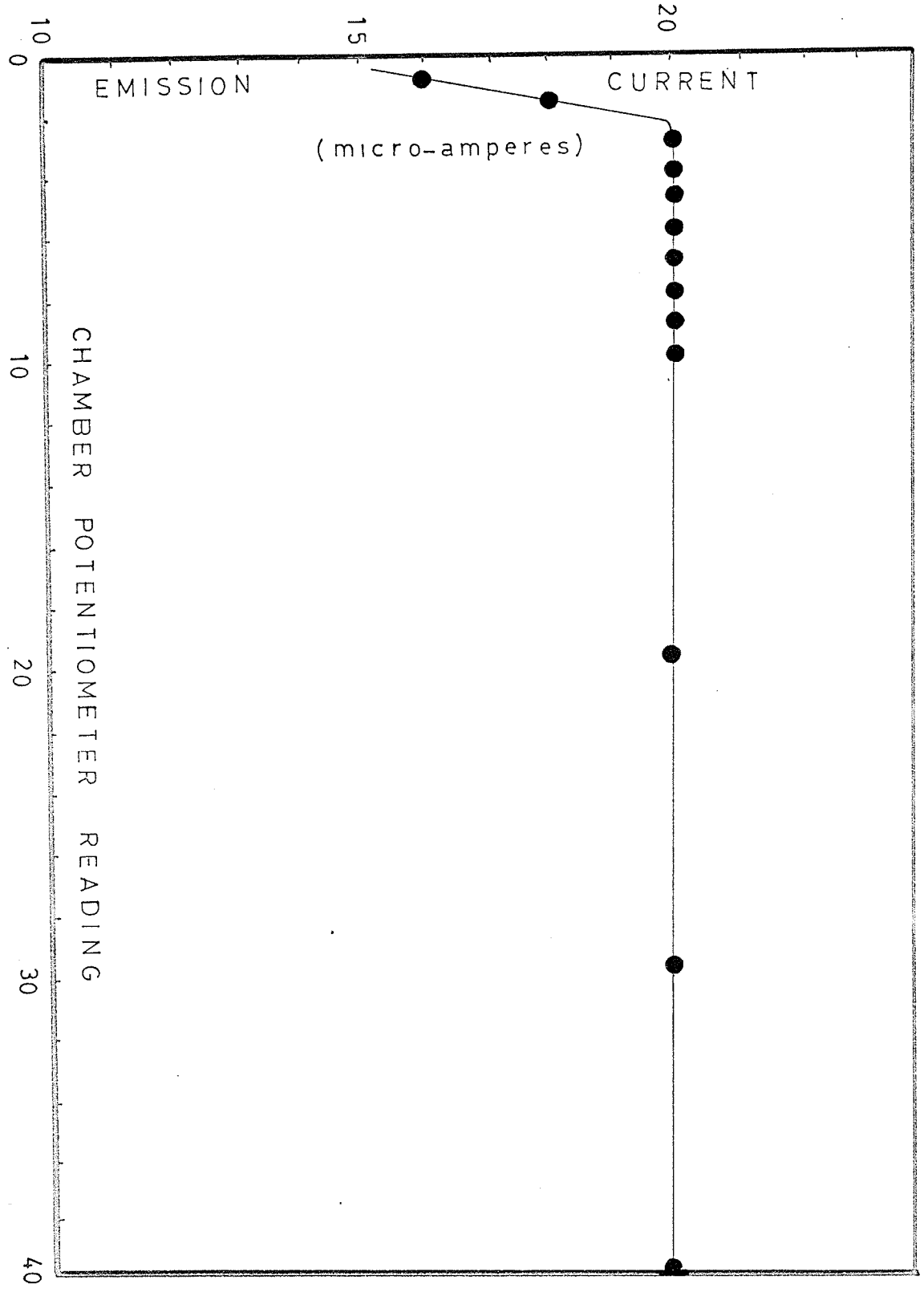
10
15
20
0
EMISSION
CURRENT
(micro-amperes)
10
20
30
40
CHAMBER POTENTIOMETER READING

FIGURE FIFTEEN

VARIATION OF THE ELECTRON ENERGY
WITH THE TOTAL EMISSION CURRENT

CONDITIONS:

Chamber Voltage: set initially at 10 volts for an emission of 50 micro-amperes
Target Voltage: 44 volts above chamber
Grid Voltage: -2 volts
Ion Acceleration Voltage: 1800 volts

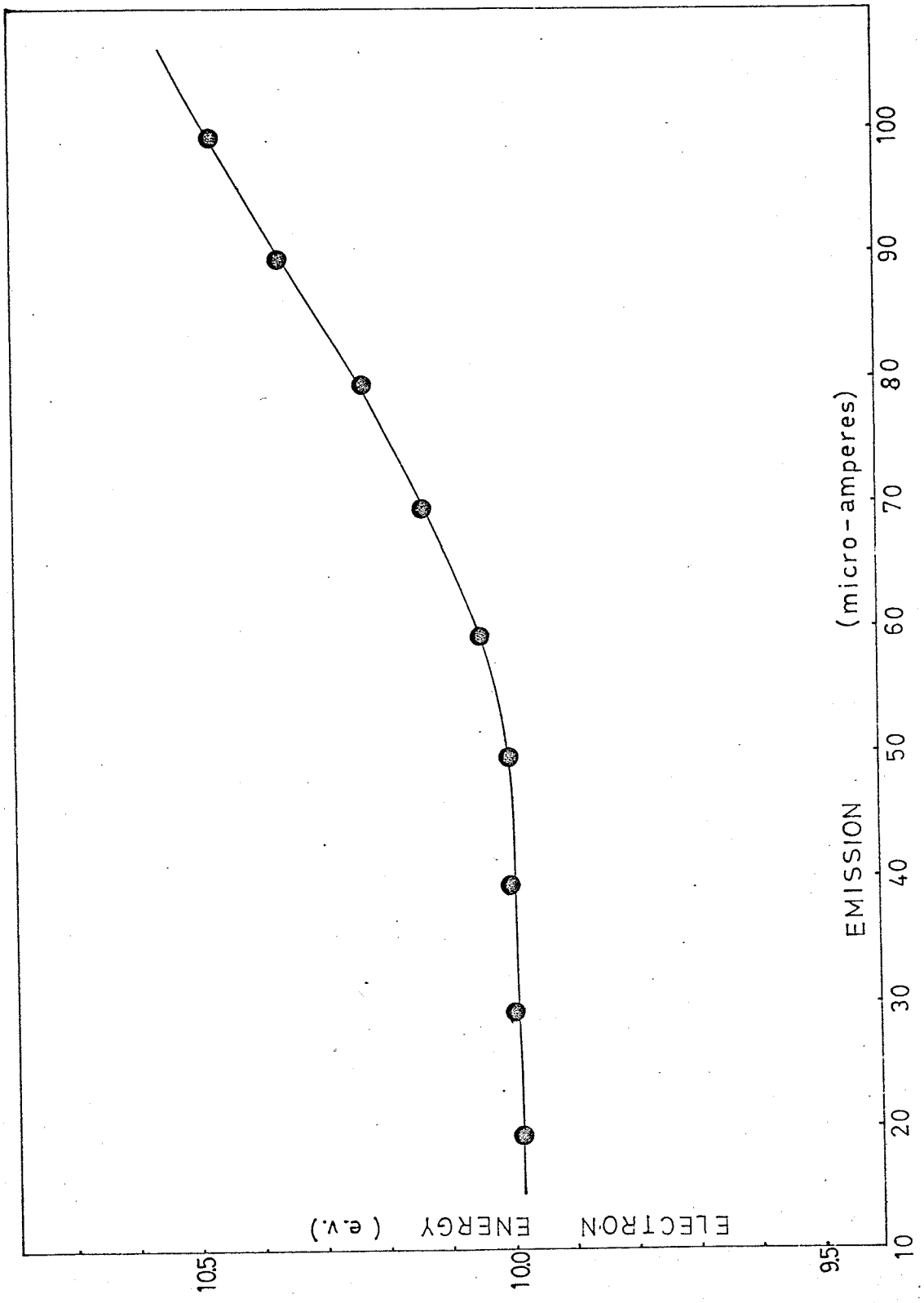
ELECTRON ENERGY (e.v.)
10.5
10.0
9.5
EMISSION (micro-amperes)
10
20
30
40
50
60
70
80
90
100

point, the energy remains fairly constant. Adjusting the chamber potentiometer to the same position each time, therefore, does not insure that the electron energy will be the same, unless the same emission is used. Note that changing the electron energy by varying the chamber voltage potentiometer and leaving the emission potentiometer constant does not affect the total emission current (figure 13); however, the converse is not true - changing the total emission potentiometer does change the chamber voltage when the chamber potentiometer is set at a fixed value (figure 15).

As illustrated in figure 16, the electron energy also has a slight dependence on the grid voltage. Once again, the emission was just stabilized at 50 micro-amperes at a chamber potential of 10 volts and a grid setting of -2 volts. Although the change in the electron energy is not as great as the change observed when the emission is varied, it is still significant (about 0.2 e.v. for a change of 7 volts in the grid potential), implying that the grid voltage must be maintained constant.

In the above measurements, an external potentiometric circuit was used to measure the electron energy as the meter on the face of the mass spectrometer was found to be insensitive to small changes in the chamber voltage. Accordingly, the meter can only be used for a qualitative estimate of the chamber voltage (and, hence, the electron energy). Besides the above experiments, the target voltage was varied over a wide range of conditions of the emission current and grid voltage. It was found to have little or no effect on either the ion intensity or the electron energy.

FIGURE SIXTEEN

VARIATION OF THE ELECTRON ENERGY
WITH THE GRID POTENTIAL

CONDITIONS:

Emission Current: 50 micro-amperes
Target current: approx. 10% of emission
Target voltage: 44 volts above chamber
Chamber voltage: set initially at 10 volts for a grid potential of -2 volts
Ion accelerating potential: 1800 volts

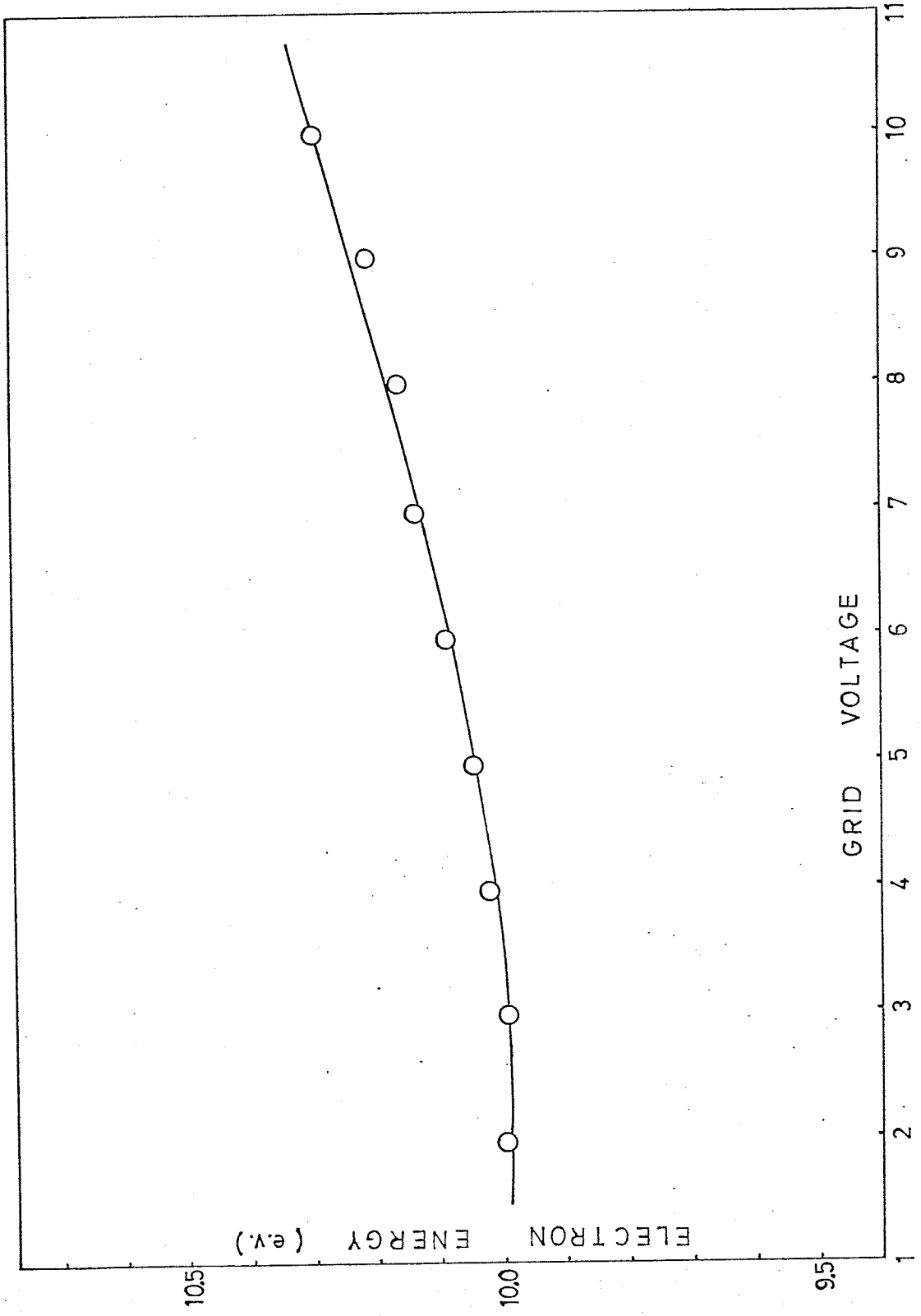
ELECTRON ENERGY (e.v.)
10.5
10.0
9.5
GRID VOLTAGE
1
2
3
4
5
6
7
8
9
10
11

To obtain an ionization efficiency curve for a negative ion, the adjustments on the RMU 6-D must be somewhat modified. When the ion optics are reversed (negative to positive) it becomes necessary to re-adjust the repeller and lens electrodes until the negative ions can be seen. It is important that the chamber voltage be set at a point where the particular negative ion will be formed from the ionizing electrons. Therefore, several positions of the chamber voltage potentiometer must be tried while the voltages on the repeller and lens electrodes are adjusted. If the ion is formed by a resonance or electron capture process, then the reaction will only occur over a very narrow range of electron energy.

Once the negative ion has been found, and the appropriate adjustments been made, the ionization efficiency curve can be obtained. Figure 17 illustrates the ionization efficiency curves for the formation of O^- from a mixture of CO and O_2. The first two peaks on the left in figure 17 represent the two electron-capture processes:

$$O_2 + e = O + O^- \qquad (a)$$

and

$$CO + e = C + O^-. \qquad (b)$$

The next rise in the curve (at about 19 e.v.) corresponds to the two ion-pair production reactions:

$$O_2 + e = O^+ + O^- + e \qquad (c)$$

and

$$CO + e = C^+ + O^- + e. \qquad (d)$$

Hagstrum(34), using a mono-energetic electron beam, has measured the appearance potential of reaction (a) as 6.5 e.v. and of reaction (b) as 9.3 e.v. Using the RMU 6-D, reaction (b) has an experimental threshold potential of about 10.2 e.v., while the end point of reaction (a) is somewhat doubtful.

FIGURE SEVENTEEN

THE IONIZATION EFFICIENCY CURVES
OF O^- FROM CO AND O_2 SHOWING
THE ELECTRON CAPTURE AND ION-PAIR
PRODUCTION PROCESSES

CONDITIONS:

Emission Current: 50 micro-amperes
Target Current: approx 10% of emission
Target Voltage: 44 volts above chamber
Grid Voltage: -2 volts
Ion Accelerator Voltage: 1800 volts

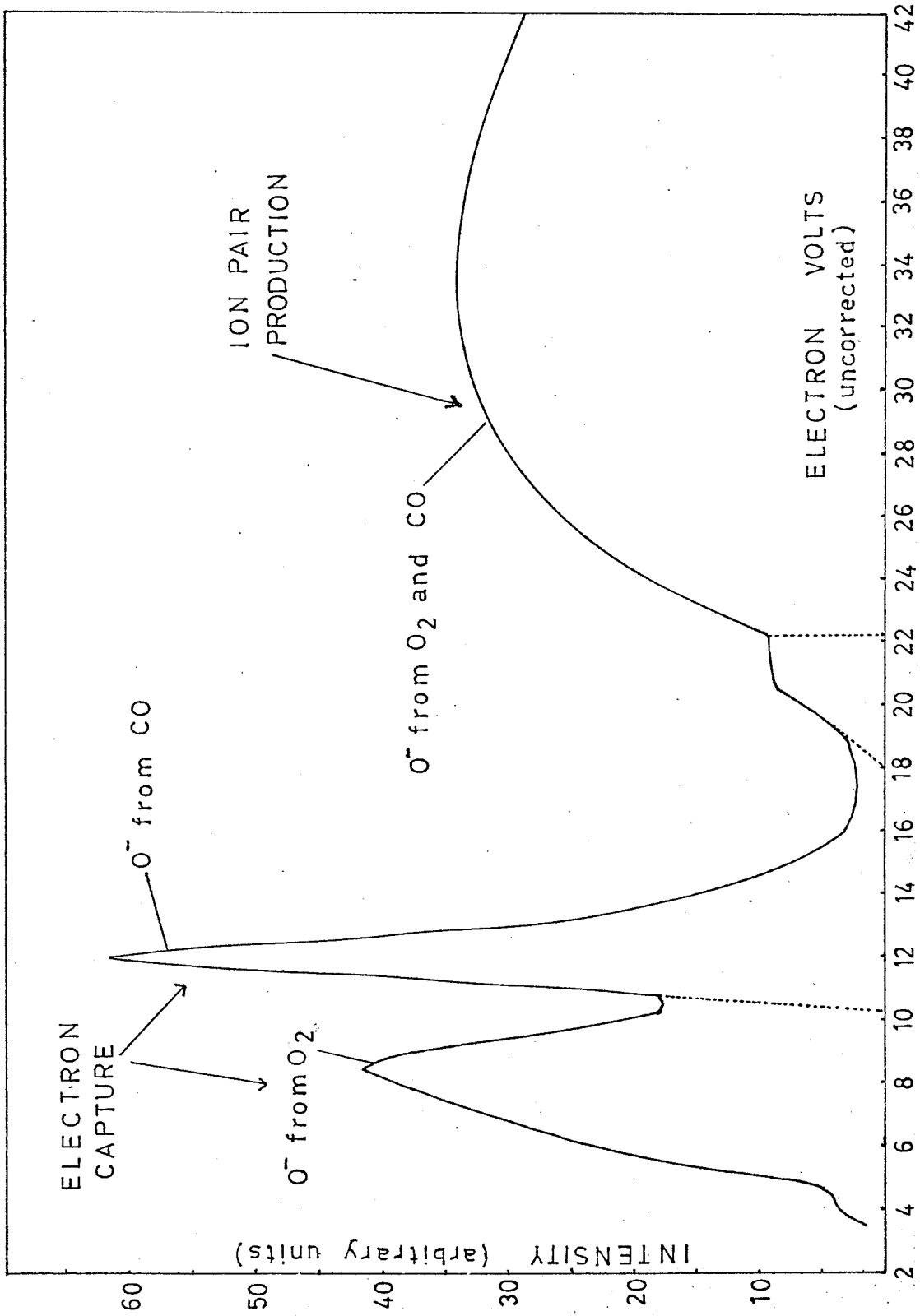
ELECTRON CAPTURE
O⁻ from CO
O⁻ from O2
ION PAIR PRODUCTION
O⁻ from O2 and CO
ELECTRON VOLTS (uncorrected)
INTENSITY (arbitrary units)
2
4
6
8
10
12
14
16
18
20
22
24
26
28
30
32
34
36
38
40
42
10
20
30
40
50
60

Reaction (c) is reported as having an appearance potential of 18 e.v. with a distinct break in the curve at 22.5 e.v., while reaction (d) should commence at 21.5 e.v. Although the two reactions undoubtably tend to obscure each other, figure 17 does indicate an extrapolated appearance potential for the pair-production process at about 18 e.v. and a corresponding break in the curve at 22.2 e.v., which agree well with Hagstrum's results for reaction (d) [34].

As an ionization efficiency curve can take from two to four hours to be obtained, there will be some decrease in the pressure of the sample. This can be corrected for in the following way. The rate of decrease of the ion current due to the pressure drop-off can be written (Graham's Law):

$$\frac{dI}{dt} = -kI/[(m)^{1/2}]$$

where m is the mass of the parent species effusing through the orifice, I is the ion current, and k is an instrumental constant. Integrating from time = 0 seconds to time = t seconds, the expression becomes:

$$\text{Log } I_o = \text{Log } I + kt/(m)^{1/2}$$

or

$$I_o = I \cdot \exp[kt/(m)^{1/2}]$$

where I_o is the value of the ion current if it were measured at the start of the ionization efficiency curve determination.

Figure 18 shows the relationship between time and the logarithm of the ion current for m/e 44, a fragment formed in the electron-impact study of PF_3. From the slope of the plot in figure 18, k has the value 1.33×10^{-3}. Hence, the expression becomes:

FIGURE EIGHTEEN

PLOT OF THE EXPONENTIAL DECREASE
OF THE ION CURRENT OF PF_3^{++} (M/E 44)
WITH TIME

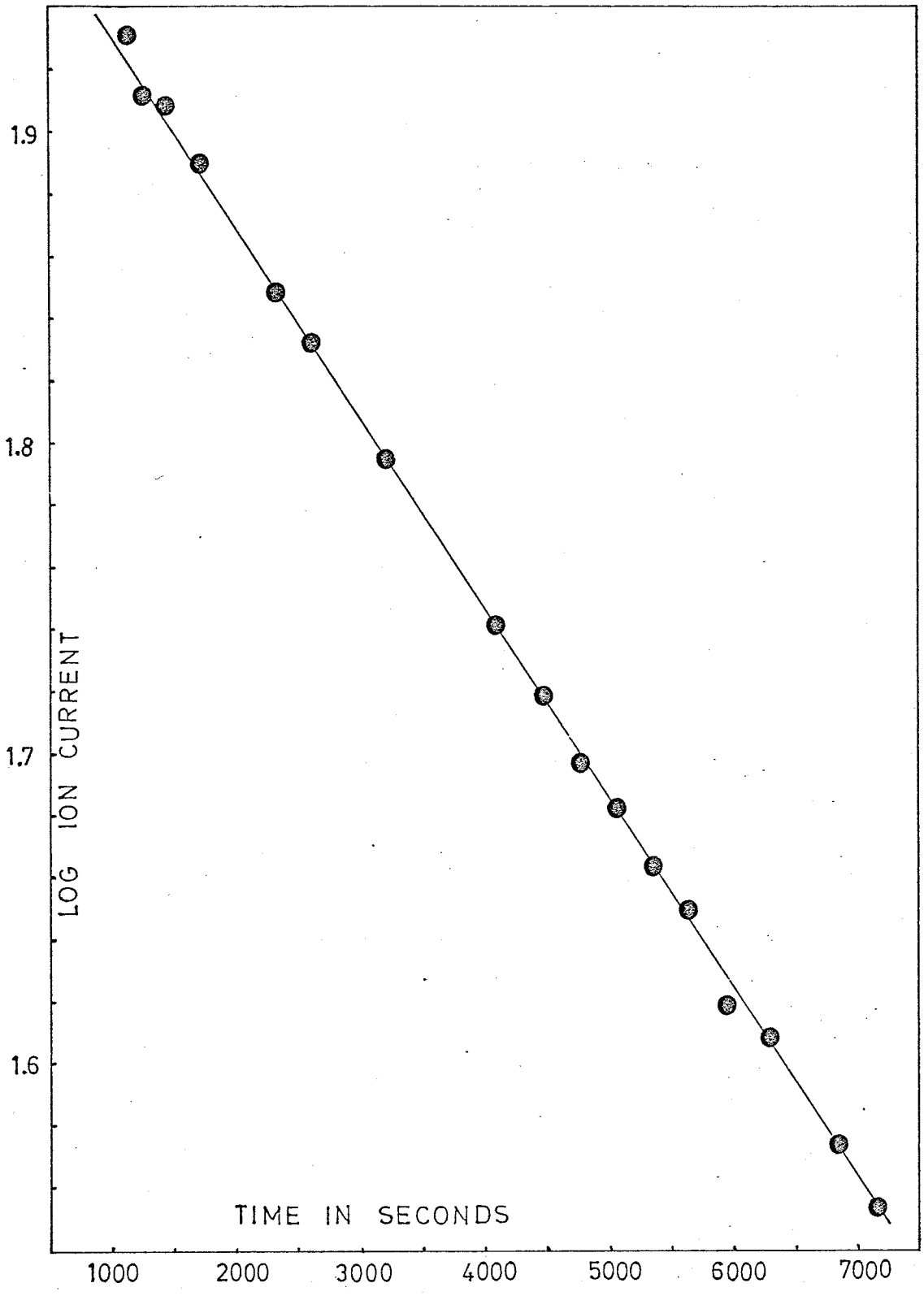
1.9
1.8
1.7
1.6
LOG ION CURRENT
TIME IN SECONDS
1000
2000
3000
4000
5000
6000
7000

$$I_o = I \cdot \exp[(1.3333 \times 10^{-3} \times t)/(m)^{1/2}].$$

Multiplying each value of the ion intensity by the appropriate factor $\exp[(1.3333 \times 10^{-3} \times t)/(m)^{1/2}]$, where t is the time in seconds from the beginning of the measurements, it is possible to correct for the fall in pressure.

Besides the pressure correction, the ionization efficiency curve data must be corrected for galvanometer sensitivity ratios and then normalized at an electron energy of 50 e.v. (if the Lossing, Tickner, and Bryce[30] method to obtain appearance potentials is being used). This is accomplished by analysing the data in the I.B.M. 1620 computer according to the FORTRAN program given in figure 18-b. The symbols used in the program are identified on the preceding page. Once the ion intensity peak heights have been measured, the data is transfered onto I.B.M. data cards according to the format in statement 7. The corresponding electron energies are transfered onto cards according to statement 5. The only adjustments required involving the object program is to fill in the DIMENSION statement subscripts and to place the appropriate integers in front of the FORMAT components in statement 6. For example, if 3 ionization efficiency curves are being determined and each consists of 99 ion intensity points, then the Dimension statement would read

```
DIMENSION U(99,3),E(99,3),X(99,3),V(3),M(3),L(3),W(3)
```

while statement 6 would be

```
6 FORMAT (7I4,6F4.1,F5.1,I2,I3).
```

An explanation of the statements used in the program can be found in any elementary FORTRAN text[35].

FIGURE EIGHTEEN-b

FORTRAN PROGRAM FOR ANALYSING
IONIZATION EFFICIENCY CURVE DATA

DEFINITION OF TERMS:

N = total number of ion intensity peaks

M = number of ion intensity peaks measured on most sensitive galvanometer

L = number of ion intensity peaks measured on second most sensitive galvanometer

W = molecular weight of the parent molecule

A = m/e value of the ion

S = time required for each scan (seconds)

K = total number of ionization efficiency curves to be analysed

IA = subscript of the ion intensity peak to be taken as the 100.00 percent value

V(I) = electron energy (e.v.)

X(I,J) = ion intensities as measured from peak heights

E(I,J) = intermediate storage of ion intensities for normalization in final Do loop

U(I,J) = normalized and corrected (pressure and galvanometer sensitivities) ion intensities

I,J = variable subscripts

```
ZZJOB 5                    2400065G          D.  TORGERSON

ZZFORX52

      DIMENSION U( , ),E( , ),X( , ),V( ),A( ),M( ),L( ),W( )
      READ 6,N,M,L,W,A,S,K,IA
    6 FORMAT (_I4,_F4.1,_F5.1,I2,I3)
      READ 5,V
    5 FORMAT (16F5.2)
      READ 7,X
    7 FORMAT (11F7.2)
      J = 1
    8 C = SQRTF(W(J))
      T = 0.0
      DO  77  I = 1,N
      IF (X(I,J)) 22,22,33
   22 E(I,J) = X(I,J)
      GO TO 44
   33 AB = .001333*T
      AC = AB/C
      D = EXPF(AC)
      IF (I-M(J)) 9,9,10
   10 IF (I-L(J)) 11,11,12
    9 XA = X(I,J)
      GO TO 13
   11 XA = X(I,J)*3.04
      GO TO 13
   12 XA = X(I,J)*26.84
   13 E(I,J)*= XA*D
   44 T = T+S
   77 CONTINUE
      DO 40  I = 1,N
      U(I,J) = (E(I,J)/E(IA,J))*100.00
      IF (I-1) 25,25,50
   25 PUNCH 17,A(J)
   17 FORMAT (6HM/E = ,F6.1/7X,13HNORM. PK. HT.,9X,13HENERGY (E.V.))
   50 PUNCH 18,U(I,J),V(I)
   18 FORMAT (9X,F7.2,15X,F6.2)
   40 CONTINUE
      J = J+1
      IF (K-J) 66,8,8
   66 CALL EXIT
      END
```

THE ELECTRON-IMPACT STUDY OF PF_3

ELECTRON-IMPACT STUDY OF PF_3

A. PHYSICAL CONSTANTS AND CHEMICAL PROPERTIES OF PF_3

PF_3 is a non-fuming, highly toxic, colourless gas with a melting point of -151.5 ± 0.2°C and a boiling point of 101.15 ± .05 °C(36). Its structure, as determined by Raman spectroscopy(37) and by electron diffraction(38,39) is trigonal pyrimidal (C_{3v} group), the P-F bond distance being given as 1.53 A° (40), 1.52 ± .04 A° (38), and 1.56 ± .02 A° (37,39). The F-P-F bond angle has been measured as 99° (37), and 99 ± 4° (39), while the P-F bond energy is 117 kilocaleries per mole(41).

Booth and Bozarth (36) have measured the heat of vaporization to be 3489 calories per mole with the vapor pressure being given by Log p = 7.310 - 761.4/T (p = vapor pressure, T = absolute temperature). Using the ideal gas approximation and statistical mechanics. Potter and DiStephano (42) have calculated, from spectroscopic data, the heat of formation of PF_3 at 0°K and at 298°K to be -220,600 calories per mole and - 221,950 calories per mole respectively. Also from spectroscopic data, Humphries, Walsh, and Warsop(43) have obtained a lower limit on the adiabatic ionization potential for PF_3 of 10.97 e.v. The difference between the adiabatic and vertical ionization potentials is about 0.7 e.v. (43). Therefore, the appearance potential of the PF_3 ion should be in the vicinity of 11.7 e.v.

PF_3 is only slowly absorbed by water but will dissolve rapidly in aqueous base(44). Water slowly decomposes PF_3 to form HF and phosphorous acid, while at high temperatures, PF_3 rapidly attacks silica(45). Most of the chemistry of PF_3 involves its ability to complex with transitional metals. These compounds are usually prepared

by substituting PF_3 for an existing ligand (such as CO) in a metal complex, either by U.V. radiation or by employing high temperatures and pressures (46,47).

B. PREPARATION

PF_3 is usually prepared from the action of a metal fluoride on PCl_3. It has been made by the direct action of PCl_3 on SbF_3 (35), CuF_2 (44), AsF_3 (45), ZnF_2 (48), and indirectly by adding PCl_3 to a solution of NaF and tetramethyl sulphone (49).

To obtain very pure PF_3 for use in the mass spectrometer, it was found that organic solvents (such as tetrahydrofuran) could not be used due to the large number of organic ion peaks that appeared in the mass spectrum. Therefore, PCl_3 (Mallinckrodt analytical reagent) was reacted directly with technical grade SbF_3 (Fisher Chemical) under vacuum, simply by condensing the PCl_3 onto the antimony trifluoride with liquid nitrogen. Only the first gases evolving from the reaction were used as samples, and these were purified principally to remove PCl_3 by passing the gas through several CO_2-acetone or CO_2- isopropanol traps. The PF_3 samples were then stored in pyrex bulbs until used up in the mass spectrometer.

C. MASS SPECTRUM OF PF_3

Figure 19 shows the mass spectrum of PF_3 at an electron acceleration potential of 70 volts. The mass spectrum has been corrected for background and the peaks due to Nitrogen (m/e 28,14), Oxygen (m/e 16,8), and H_2O(m/e 16,17,18) have been removed. The pattern coefficent of PF_3 is greatly simplified due to the fact that both phosphorus and fluorine

FIGURE NINETEEN

THE MASS SPECTRUM OF PF_3

CONDITIONS

Chamber Voltage: 70 volts
Target Voltage: 44 volts above chamber
Emission Current: 81 micro-amperes
Target Current: 35 micro-amperes
Ion Acceleration Voltage: 3600 volts

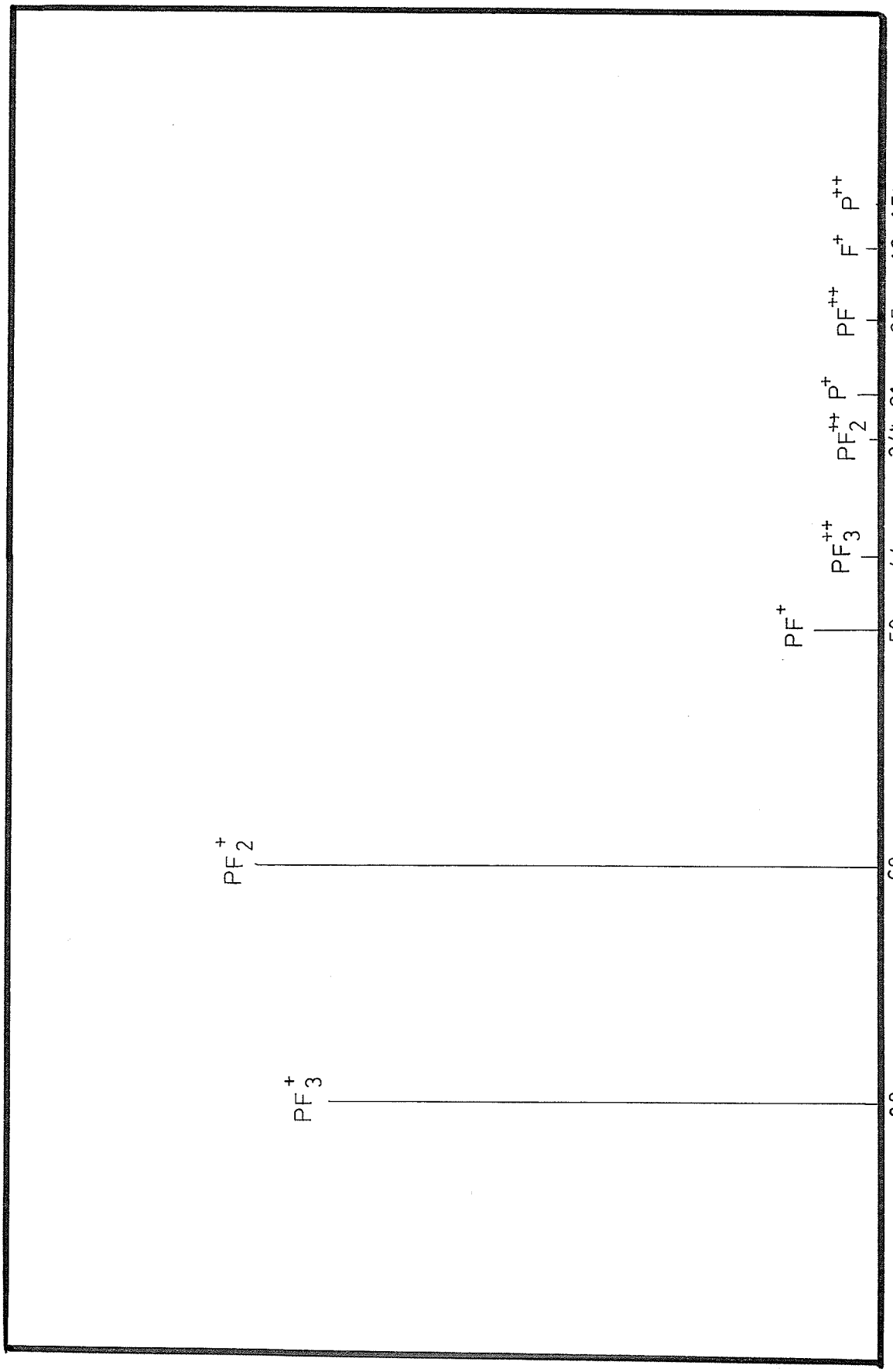
PF_3^+
88
PF_2^+
69
PF^+
50
PF_3^{++}
44
PF_2^{++}
34½
P^+
31
PF^{++}
25
F^+
19
P^{++}
15½

are anisotopic - hence only 10 ions were observed. In addition to these, peaks that varied greatly in intensity from sample to sample were observed at m/e 104, 85, 81, 38, 36, 35, and 20. The m/e 104 and 85, peaks are due to SiF_4^+ and SiF_3^+, respectively and arise, presumably, from the attack of PF_3 on the glass sample bottles(45). The HCl at m/e 38 and 36, and the Cl at m/e 35 and 37 are byproducts of the SbF_3 - PCl_3 reaction, the HCl being formed from the H_2O impurities in the SbF_3. The m/e 20 peak, due to HF, arises from the reaction of H_2O and PF_3(44). The m/e 81 peak, which varied in intensity more than any other peak, was not identified. The pattern coefficients of PF_3 at 50 and 70 volts are presented in table I (corrected for background).

D. THE IONIZATION POTENTIAL OF PF_3

The ionization potential of PF_3 was determined using three of the procedures discussed in the introduction: (1) the Warren "extrapolated voltage difference" method(32), and (2) the Winters "energy distribution difference" method (31), and (3) the Lossing, Tickner, Bryce semilogarithmic method (30). In all, four experiments were performed with Kr as the calibrant, table II illustrating the data obtained for experiment #3. The 0.1 volt steps were measured using the external potentiometer which could be read to at least 0.005 of a volt. The unprocessed data is shown as well as the corrected, normalized data from the computer, the ΔI function for Winter's method and in the final column, the values of the adjusted Kr ion intensities used in the Warren method

TABLE ONE

PATTERN COEFFICIENTS OF PF_3
AT 50 AND 70 VOLTS

M/E	ION	50 VOLT ELECTRONS	70 VOLTS ELECTRONS
15 1/2	P^{++}	0.23	0.86
19	F^{+}	2.47	3.56
25	PF^{++}	2.47	6.90
31	P^{+}	3.34	4.31
34 1/2	PF_2^{++}	1.59	3.13
44	PF_3^{++}	2.75	3.93
50	PF^{+}	9.70	9.38
69	PF_2^{+}	100.00	100.00
88	PF_3^{+}	88.21	70.62
19	F-	(see figure 29)	

Conditions: see figure 19

TABLE TWO

DATA FOR EXPERIMENT 3

Notes: (I) change to second most sensitive galvanometer

(II) change to least sensitive galvanometer

EXPERIMENT NUMBER 3 DATA

ENERGY (e.v.)	UNPROCESSED ION INTENSITIES (mm)		NORMALIZED ION INTENSITIES (from computer)		ΔI FUNCTION = I(V)-bI(V')		WARREN VALUES for Kr
	PF_3	Kr	PF_3	Kr	PF_3	Kr	
6.00	.25						
6.10	.35						
6.20	.30						
6.30	.40						
6.40	.60		.01				
6.50	.65		,01				
6.60	.80		.02				
6.70	1.12		.02		-.01		
6.80	1.35		.02		0		
6.90	1.87		.03		0		
7.00	1.90		.03		.01		
7.10	2.95		.06		-.02		
7.20	3.44	.20	.07		-.01		
7.30	4.20	.21	.09		0		
7.40	5.70	.28	.12		0		
7.50	7.70	.20	.17		-.01		
7.60	9.10	.39	.20		.02		
7.70	11.96	.35	.27		-.01		
7.80	14.85	.40	.35		0		
7.90	18.70	.45	.44		-.01		
8.00	7.60(I)	.50	.56		-.01		
8.10	8.75	.62	.66		.05		
8.20	10.60	.72	.81		.03		
8.30	12.30	.85	.96	.01	.07	-.01	.02
8.40	14.50	.90	1.15	.01	.07	0	.02
8.50	16.60	1.10	1.33	.01	.12	0	.02
8.60	2.15(II)	1.00	1.55	.01	.13	0	.02
8.70	2.40	1.40	1.76	.02	.19	-.01	.04
8.80	2.70	1.71	2.02	.02	.20	0	.04
8.90	3.10	1.81	2.35	.02	.26	0	.04
9.00	3.40	2.20	2.63	.03	.31	0	.05
9.10	3.67	2.68	2.88	.04	.40	.01	.07
9.20	4.05	3.40	3.24	.05	.37	0	.09
9.30	4.40	3.79	3.57	.06	.48	.01	.11
9.40	4.78	3.97	3.95	.06	.51	.01	.11
9.50	5.05	5.10	4.24	.08	.67	0	.15
9.60	5.55	5.78	4.74	.10	.57	0	.18
9.70	5.90	6.79	5.12	.12	.78	0	.22
9.80	6.15	8.55	5.43	.15	.92	0	.27
9.90	6.78	10.81	6.09	.19	.72	0	.35

EXPERIMENT NUMBER 3 DATA (CONTINUED)

ENERGY (e.v.)	UNPROCESSED ION INTENSITIES (mm)		NORMALIZED ION INTENSITIES (from computer)		ΔI FUNCTION = I(V)-bI(V')		WARREN VALUES for Kr
	PF_3	Kr	PF_3	Kr	PF_3	Kr	
10.00	7.00	13.03	6.39	.24	1.15	.0	.44
10.10	7.40	15.79	6.87	.30	1.07	.0	.55
10.20	7.88	6.60(I)	7.44	.38	1.11	.0	.69
10.30	8.21	8.25	7.88	.49	1.34	-.01	.89
10.40	8.60	10.50	8.39	.63	1.39	-.01	1.15
10.50	9.07	12.79	9.00	.79	1.42	.0	1.44
10.60	9.55	15.05	9.63	.94	1.55	.04	1.74
10.70	9.95	17.76	10.20	1.13	1.74	.04	2.06
10.80	10.25	20.47	10.68	1.33	1.93	.07	2.42
10.90	10.57	23.72	11.20	1.56	2.01	.08	2.84
11.00	10.74	26.64	11.57	1.79	2.24	.13	3.26
11.10	11.24	29.65	12.31	2.02	2.04	.18	3.68
11.20	11.55	32.54	12.87	2.26	2.35	.21	4.11
11.30	11.91	36.69	13.49	2.59	2.43	.19	4.71
11.40	12.38	39.70	14.26	2.85	2.45	.31	5.19
11.50	12.79	42.74	14.97	3.12	2.67	.36	5.58
11.60	13.26	45.81	15.78	3.40	2.76	.40	6.19
11.70	13.42	50.51	16.24	3.81	3.21	.36	6.93
11.80	13.78	53.55	16.96	4.11	3.11	.53	7.48
11.90	14.19	57.65	17.75	4.50	3.22	.51	8.19
12.00	14.40	59.38	18.32	4.71	3.57	.74	8.50
12.50	16.47	80.34	21.30	6.49			11.81
12.90	18.44	97.08	24.25	7.97			14.51
13.50	21.96	127.19	29.36	10.62			19.33
13.90	23.33	138.17	31.71	11.74			21.37
15.41	27.43	19.58(II)	38.18	14.93			27.32
20.62	62.68	66.61	88.08	51.67			94.56
25.84	74.48	98.45	106.41	77.66			142.12
40.13	69.72	116.66	101.27	93.58			171.25
50.00	67.71	122.58	100.00	100.00			183.00

in order to make the linear portion of the Kr curve parallel to the linear portion of the PF_3 curve (see figure 20). These latter values were obtained by multiplying the Kr data by the ratio of the slopes of the Kr and PF_3 curves in figure 20 (1.83). The ΔV values were then obtained as shown and were plotted against the ion intensities (figure 21-A). The plot was extrapolated to zero ion current and the difference between the ionization potential of PF_3 and Kr was obtained.

Figure 21-B shows the detail of the semilogarithmic normalized plot in the regions below 1% peak intensity. The curves were found to be parallel at 0.3% intensity, at which point the difference in the ionization potentials of Kr and PF_3 was taken.

The ΔV functions were obtained by using a ΔV parameter of 0.1 volt, and by calculating b from the slopes of the exponential portions of the ionization efficiency curves. These are plotted in figure 22 for experiment three.

Table (III) indicates the results of all four experiments along with the conditions of measurement. The grid was set at -2 volts and the target voltage was 44 volts above the chamber potential for all four experiments.

E. IONIZATION EFFICIENCY CURVES OF FRAGMENT IONS

The ionization efficiency curves for the ions in the mass spectrum of PF_3 are presented in figure 23 to 29 inclusive, except for the m/e 15 1/2 ion (P^{++}) which could not be measured due to its low intensity. For the positive ions, both the semilogarithmic and

FIGURE TWENTY

EXPERIMENT NUMBER 3

THE ADJUSTING OF THE LINEAR PORTIONS OF THE Kr^+ I.E. CURVE TO BE PARALLEL WITH THE PF_3^+ CURVE

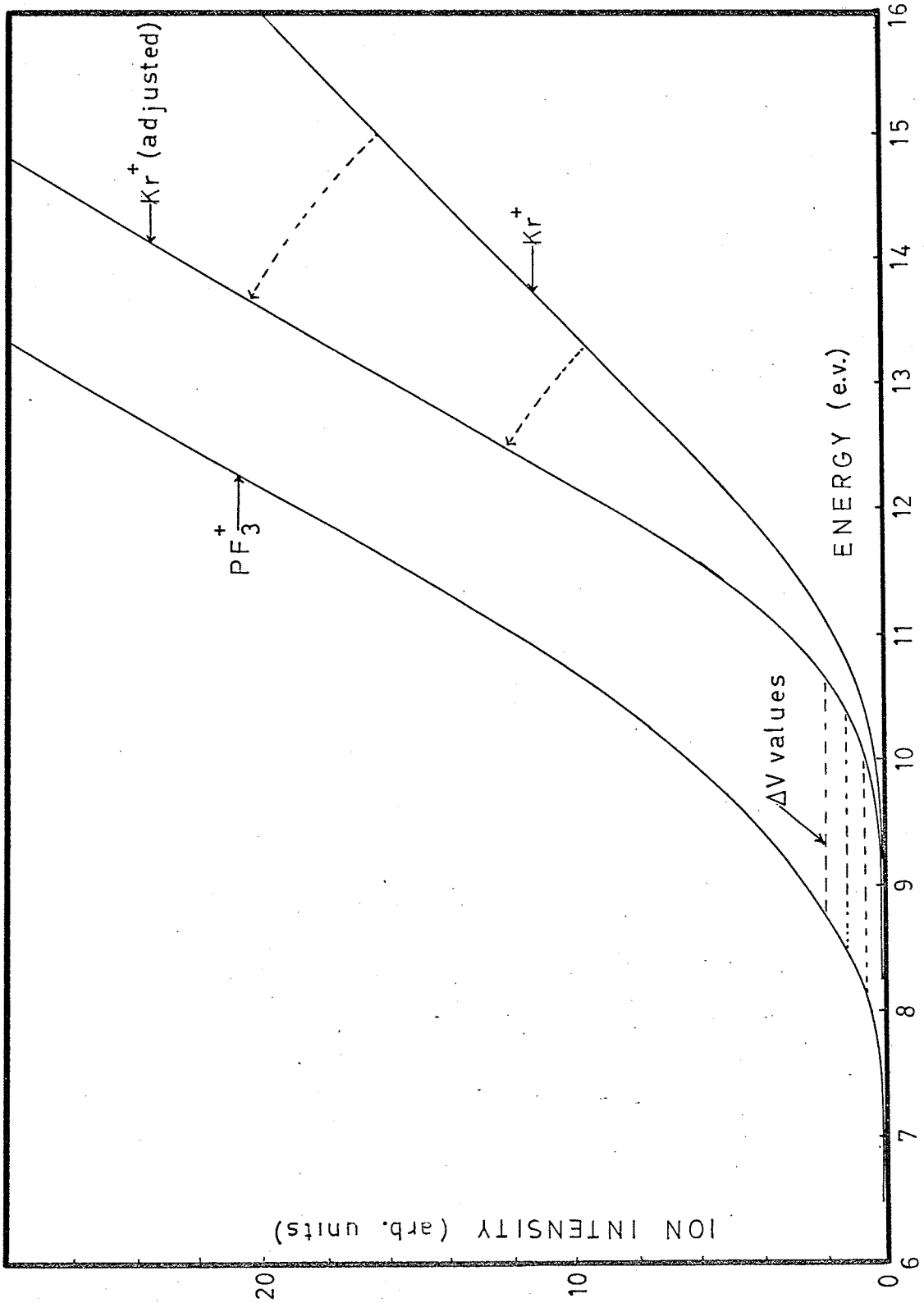
Kr^+ (adjusted)
Kr^+
PF_3^+
ΔV values
ENERGY (e.v.)
ION INTENSITY (arb. units)
6
7
8
9
10
11
12
13
14
15
16
0
10
20

FIGURE TWENTY-ONE

A. THE ΔV VERSUS ION CURRENT PLOT FOR EXPERIMENT NUMBER 3 DATA

B. DETAIL OF THE LOWER PART OF THE SEMILOGARITHMIC I.E. CURVES FOR EXPERIMENT NUMBER 3 DATA

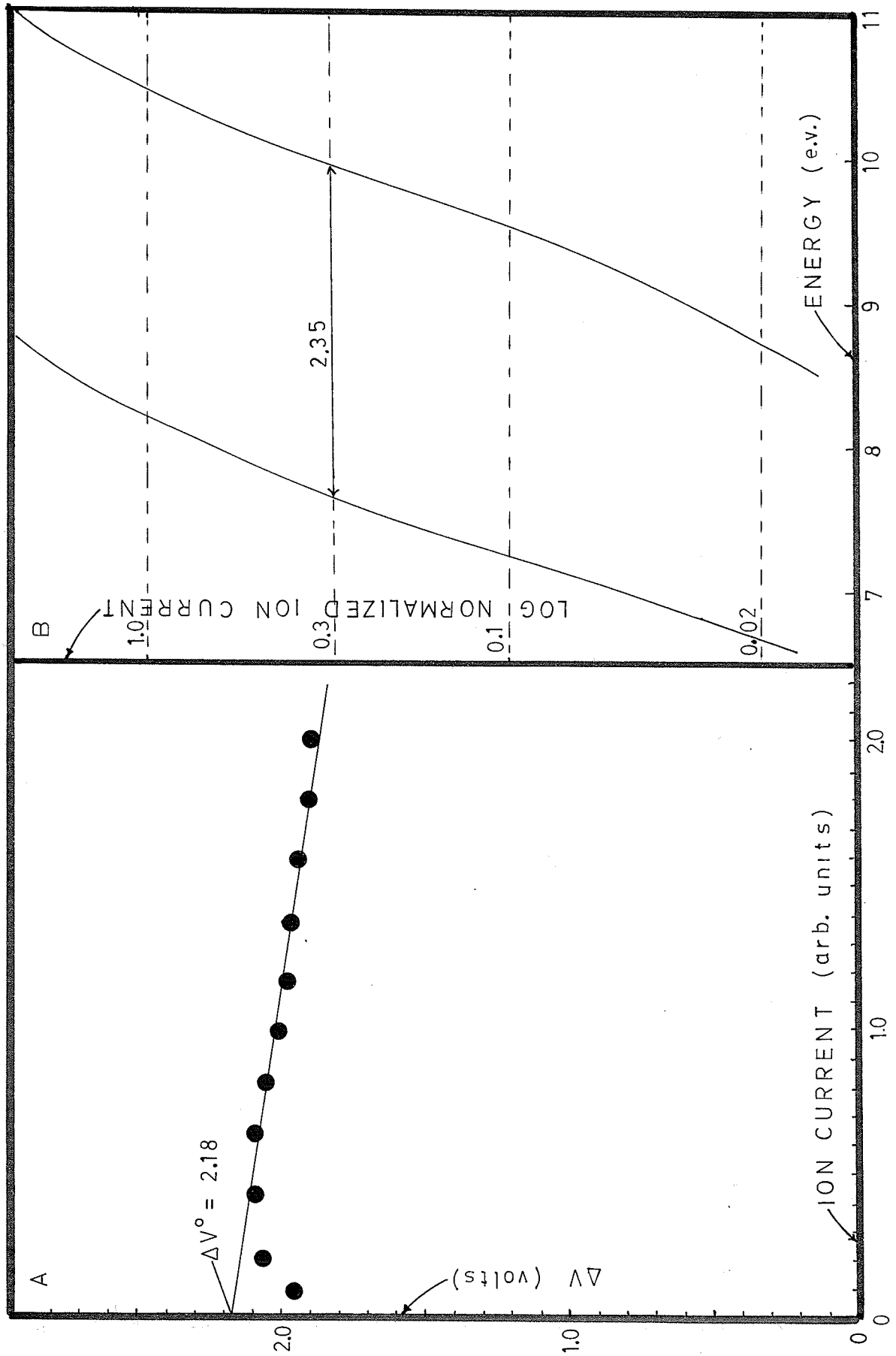
A
B
ΔV° = 2.18
ΔV (volts)
ION CURRENT (arb. units)
LOG NORMALIZED ION CURRENT
ENERGY (e.v.)
2.35
1.0
0.3
0.1
0.02
0
1.0
2.0
7
8
9
10
11

FIGURE TWENTY-TWO

ΔI FUNCTIONS FOR Kr AND
PF_3 (EXPERIMENT NUMBER 3 DATA)

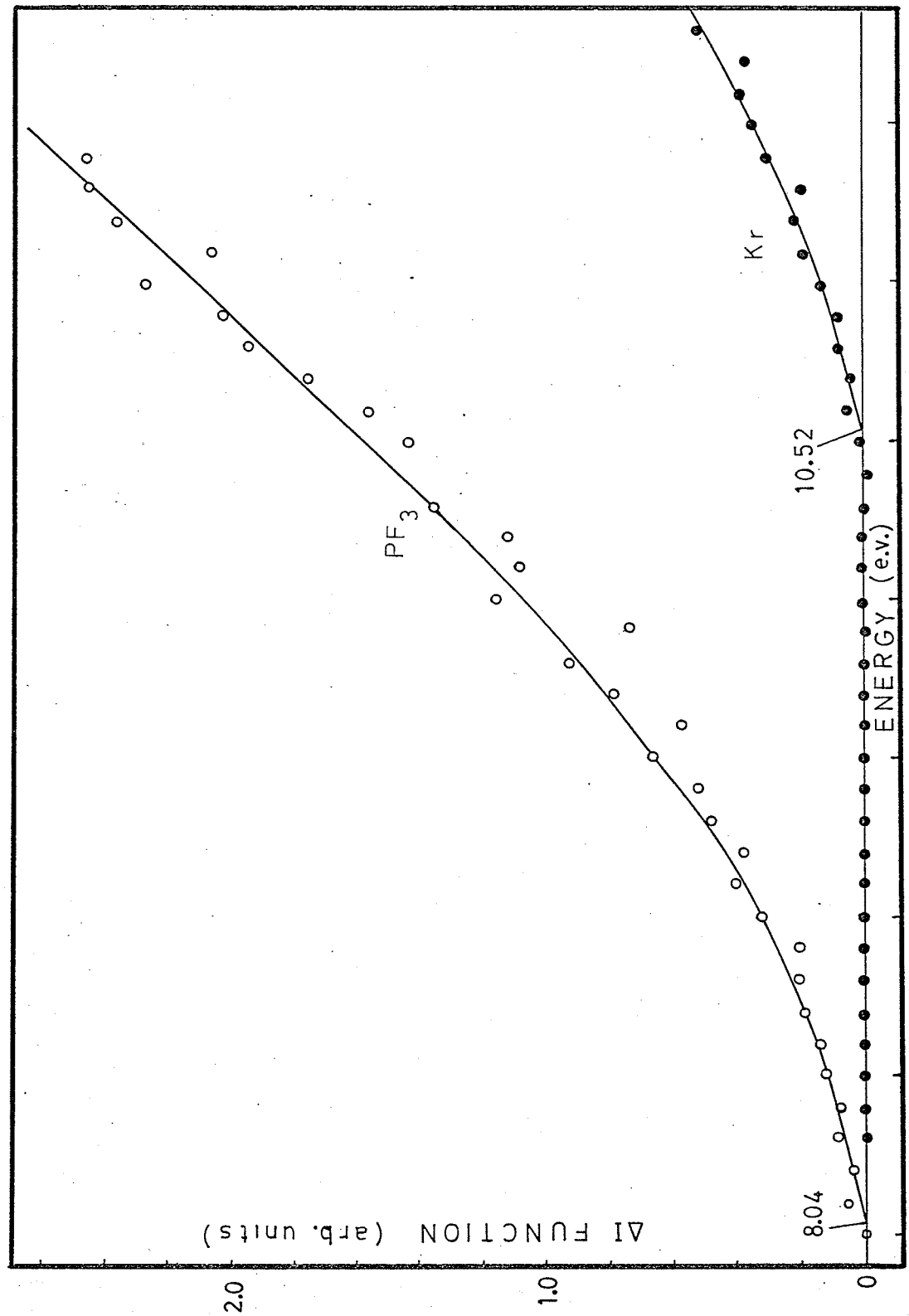
AI FUNCTION (arb. units)
2.0
1.0
0
8
9
10
11
ENERGY (e.v.)
PF_3
Kr
10.52
8.04

TABLE THREE

IONIZATION POTENTIAL OF PF_3

EXP.	EMISSION micro-amperes	ION ACCEL. VOLTS	WARREN VALUES	L.T.B. VALUES	WINTERS VALUES	STANDARDS
1	70	3600	11.72	11.64	11.78	Kr^{84}
2	70	3600	11.80	11.59	11.69	Kr^{84}
3	50	1800	11.82	11.65	11.52	Kr^{86}
4	50	1800	11.91	11.63	11.56	Kr^{86}
Average			$11.81^{+}-.06$	$11.63\pm.02$	$11.64\pm.09$	

FIGURE 23: I.E. CURVES FOR PF_3^+, Kr^+, PF_2^+

FIGURE 24: SEMILOG I.E. CURVES FOR PF_3^+, Kr^+, PF_2^+

FIGURE 25: I.E. CURVES FOR Ar^+, P^+, F^+, PF_2^{++}, PF^{++}

FIGURE 26: SEMILOG I.E. CURVES FOR Ar^+, P^+, F^+, PF_2^{++}, PF^{++}

FIGURE 27: I.E. CURVES FOR Ar^+, PF^+, PF_3^{++}

FIGURE 28: SEMILOG I.E. CURVES FOR Ar^+, PF^+, PF_3^{++}

Conditions

Target Potential: 44 volts above chamber
Emission Current: 70 micro-amperes
Target Current: approx. 60% of emission
Ion Acceleration Voltage: 3600 volts
Grid Voltage: -2 volts

Energy scales are uncorrected
Ion intensity is normalized in all cases

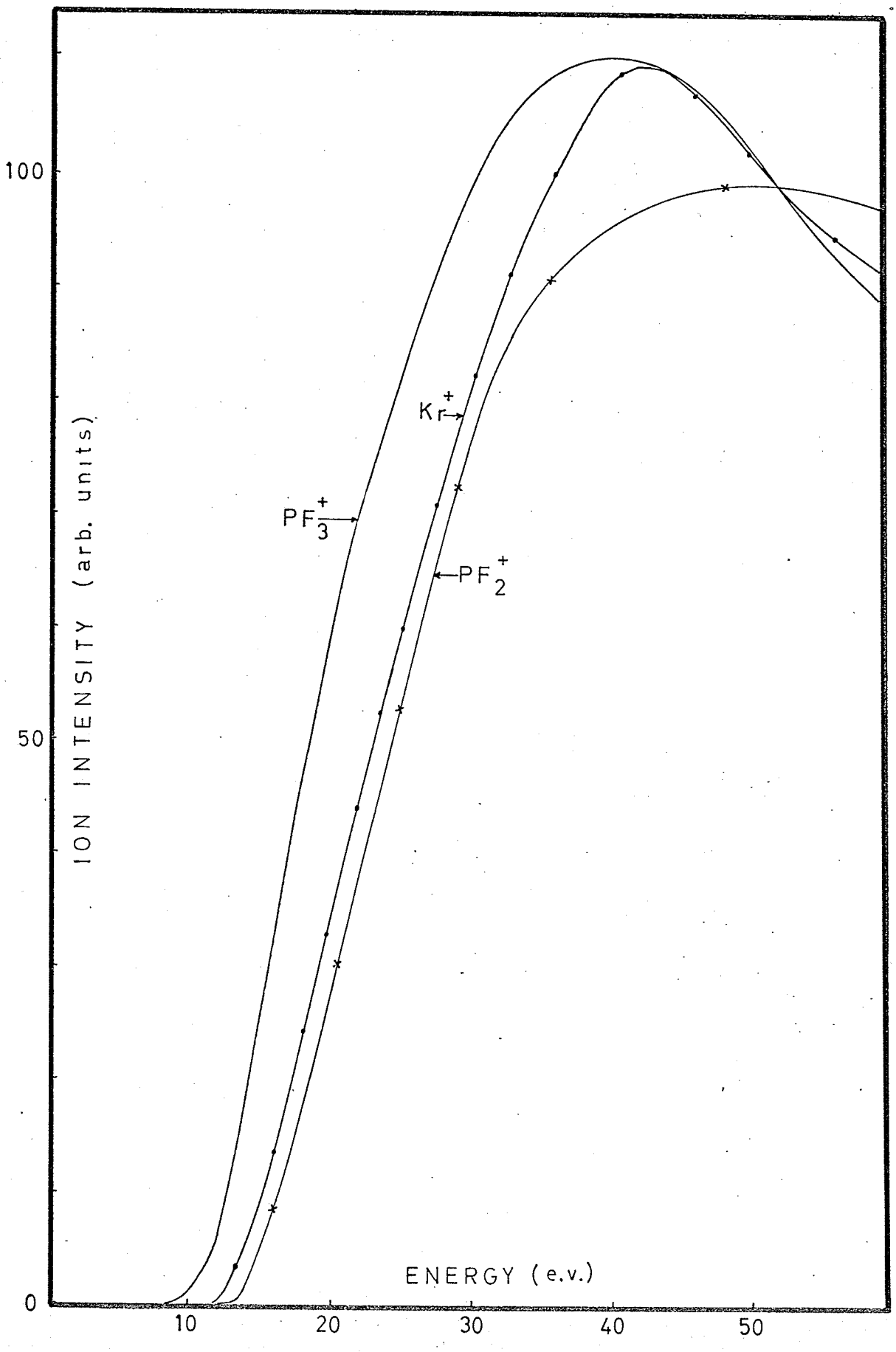
100
50
0
ION INTENSITY (arb. units)
PF_3^+
Kr^+
PF_2^+
10
20
30
40
50
ENERGY (e.v.)

FIG. 23

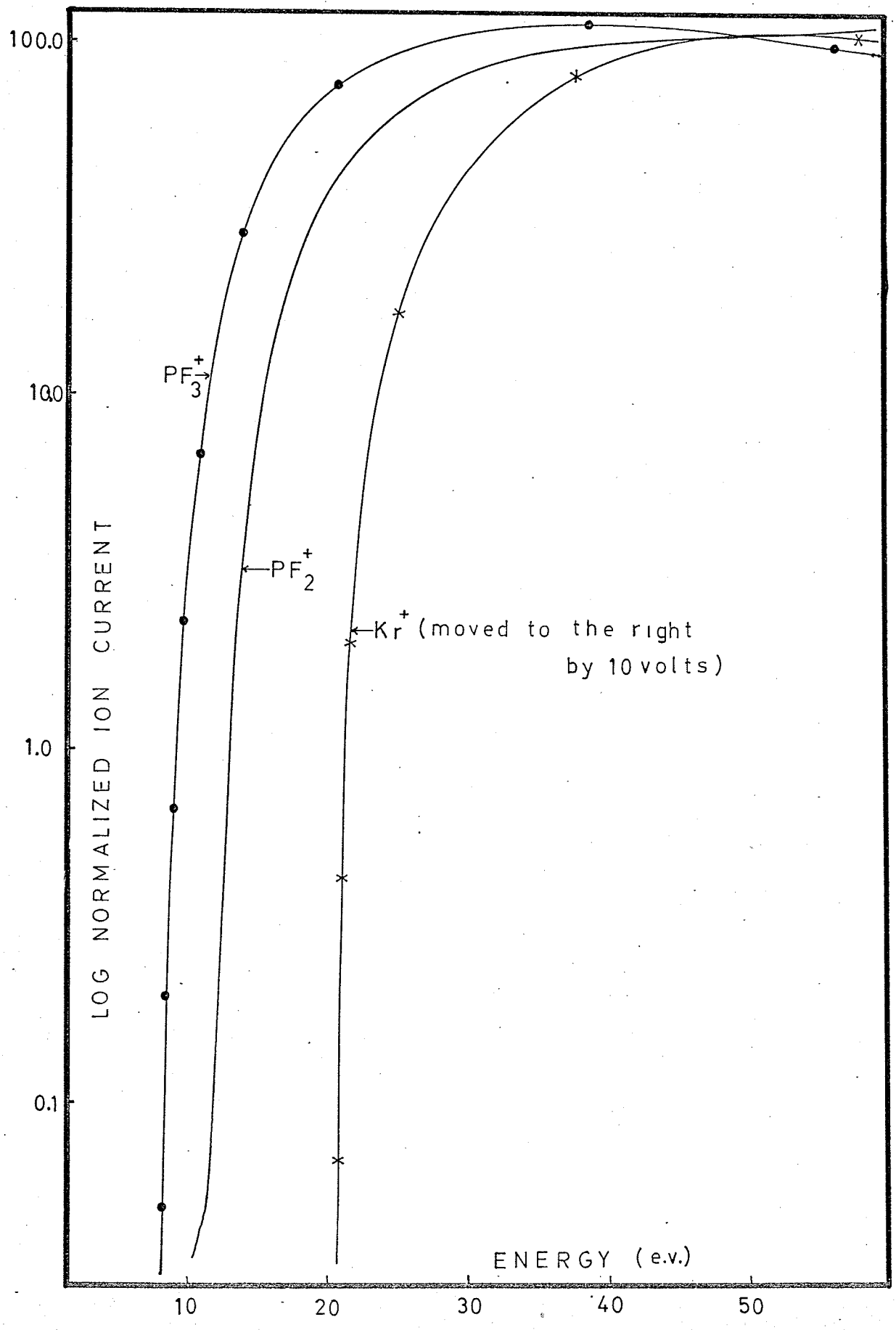
100.0
10.0
1.0
0.1
LOG NORMALIZED ION CURRENT
PF_3^+
PF_2^+
Kr^+ (moved to the right by 10 volts)
ENERGY (e.v.)
10
20
30
40
50

FIG. 24

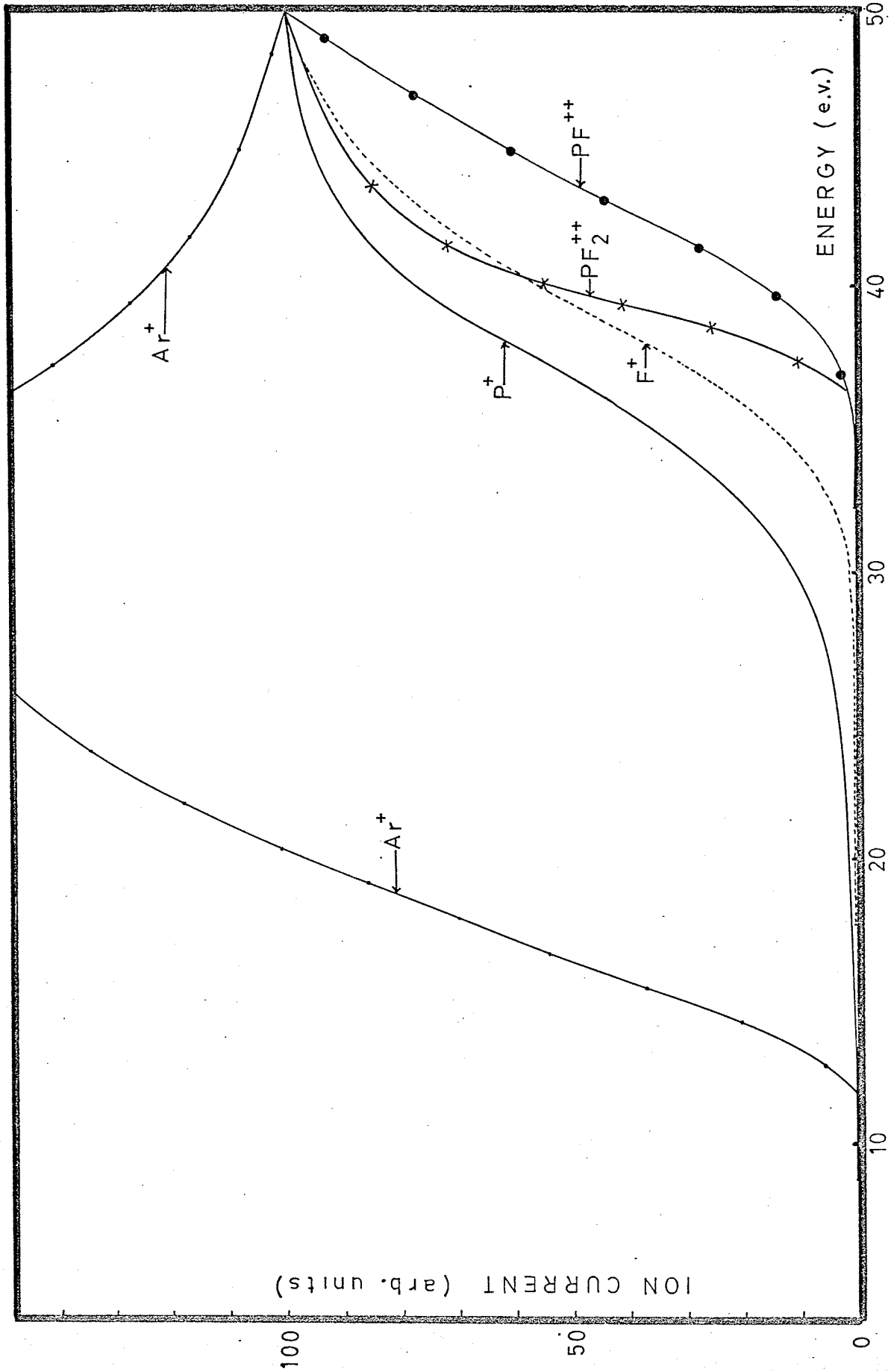
ION CURRENT (arb. units)
0
50
100
ENERGY (e.v.)
10
20
30
40
50
Ar^+
P^+
F^+
PF^{++}
PF_2^{++}
Ar^+

FIG 25

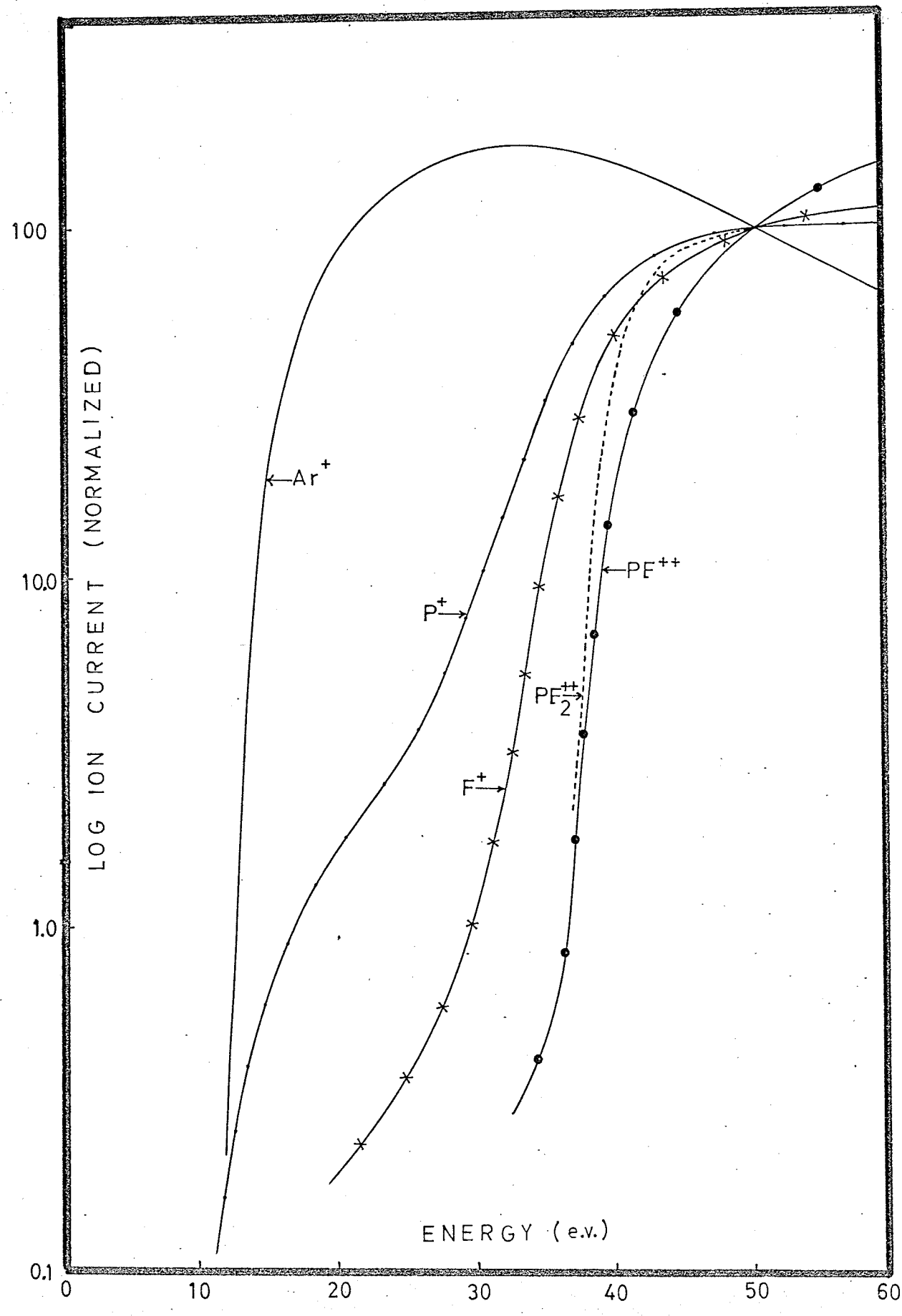
100
10.0
1.0
0.1
LOG ION CURRENT (NORMALIZED)
Ar+
P+
PF++
PF++2
F+
0
10
20
30
40
50
60
ENERGY (e.v.)

FIG 26

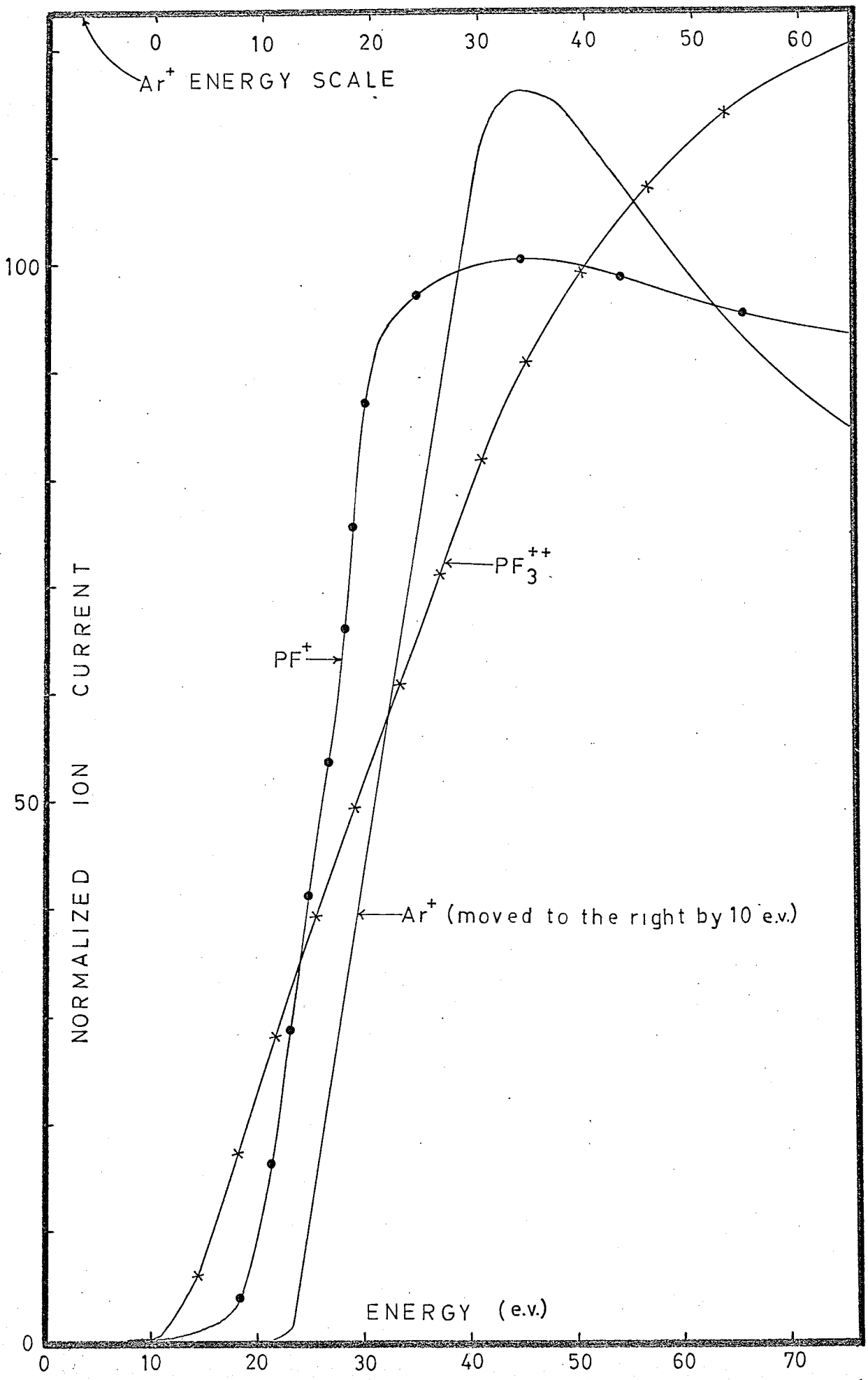
0
10
20
30
40
50
60
Ar+ ENERGY SCALE
100
50
0
NORMALIZED ION CURRENT
PF+
PF3++
Ar+ (moved to the right by 10 e.v.)
ENERGY (e.v.)
0
10
20
30
40
50
60
70

FIG 27

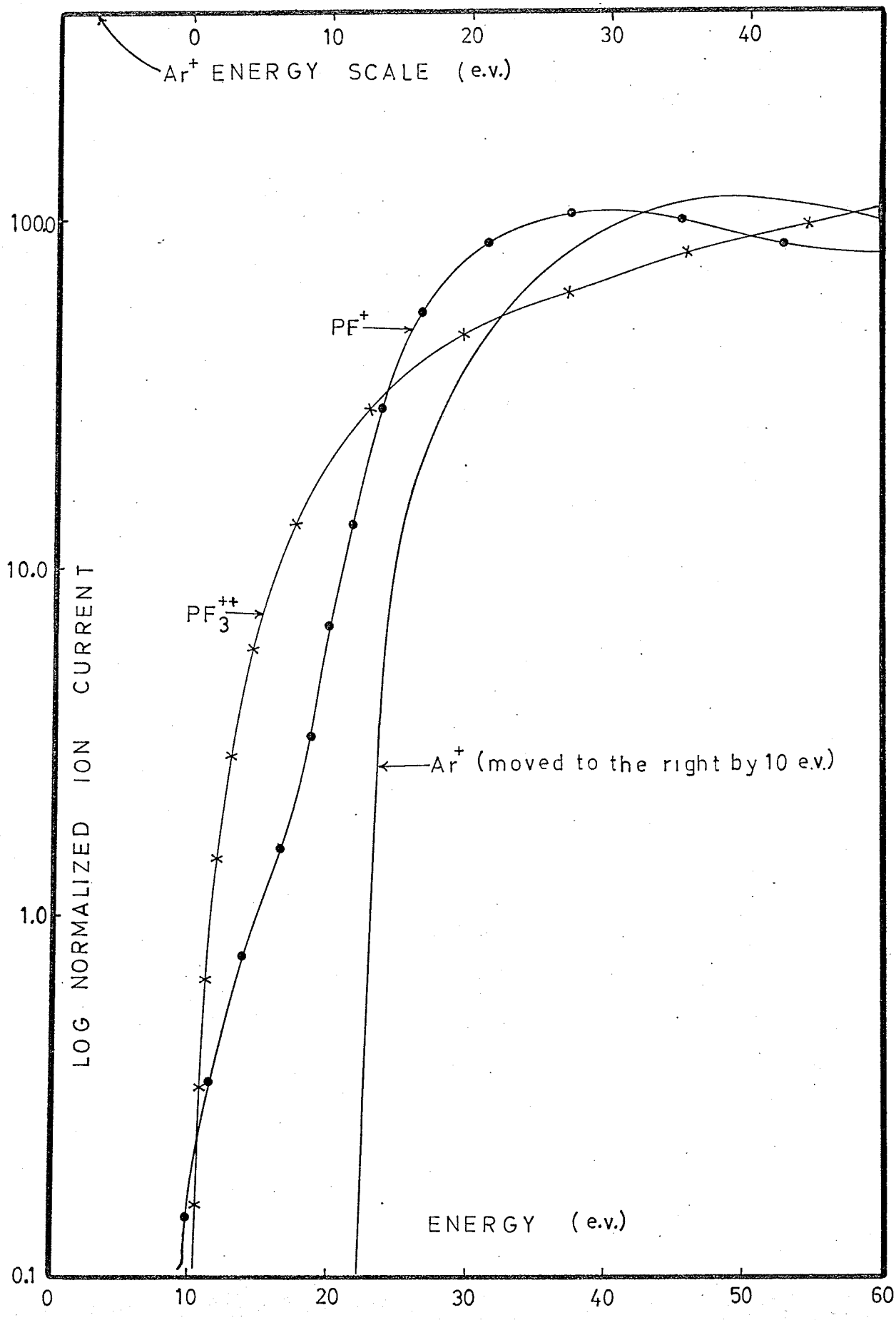
0
10
20
30
40
Ar+ ENERGY SCALE (e.v.)
100.0
10.0
1.0
0.1
LOG NORMALIZED ION CURRENT
PF+
PF3++
Ar+ (moved to the right by 10 e.v.)
ENERGY (e.v.)
0
10
20
30
40
50
60

FIG 28

FIGURE TWENTY-NINE

IONIZATION EFFICIENCY CURVE FOR F^-

Conditions

Grid Voltage: -2 volts
Emission Current: 50 micro-amperes
Target Current: approx. 10% of emission
Target Voltage: 44 volts above chamber
Ion Acceleration Voltage: 1800 volts

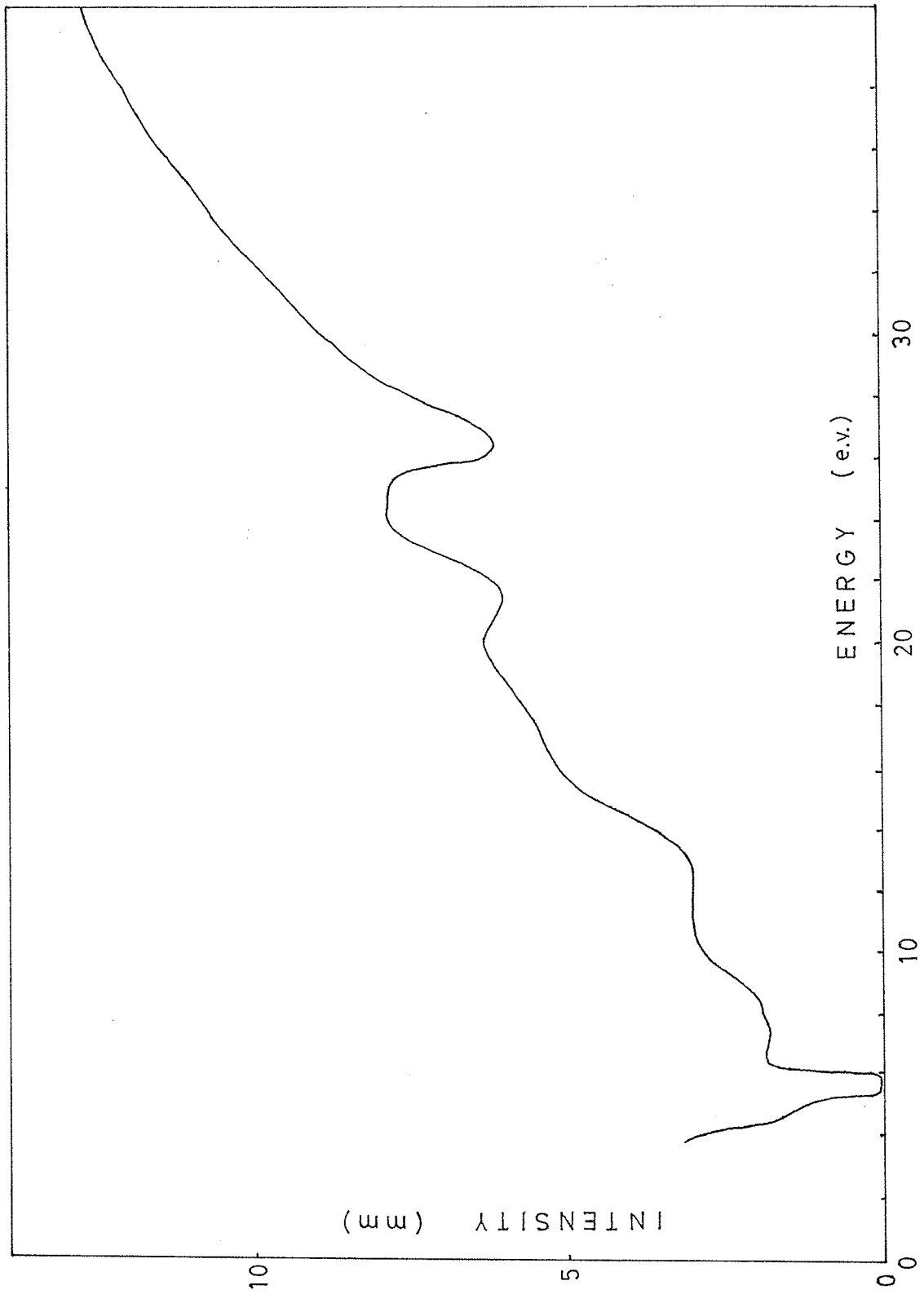
INTENSITY (mm)
0
5
10
ENERGY (e.v.)
0
10
20
30

the normal curves are given. The appearance potentials for these ions are presented in table (IV), as estimated from the ionization efficiency curves either by the Warren (W) or Lossing, Tickner, Bryce (L.T.B.) method, whichever was more convenient. Also tabulated in table(IV) are the probable processes of formation and the heats of formation for some of the ions. The ionization potential of Ar was taken as 15.76 and of Kr as 14.00(16) .

TABLE FOUR

APPEARANCE POTENTIALS OF FRAGMENT IONS AND HEATS OF FORMATION

ION	PROBABLE PROCESS	A.P. (e.v.)	METHOD USED	ΔH_f° (K.cal.)
PF_2^+	$PF_3 + e = PF_2^+ + F + 2e$	15.5	(LTB)	135
PF^+	(1) $PF_3 + e = PF^+ + 2F + 2e$ (2) $PF + e = PF^+ + 2e$ or $PF_2 + e = PF^+ + F + 2e$	20.5 12.7	(W) (LTB)	250
P^+	(1) $PF_3 + e = P^+ + 3F + 2e$ (2) $P + e = P^+ + 2e$ or $PF + e = P^+ + F + 2e$	(1) 32.3 (2)-14	(W) (LTB)	515
F^+	$PF_3 + e = 2F + P + F^+$	36.0	(W)	
PF_3^{++}	$PF_3 + e = PF_3^{++} + 3e$			
PF_2^{++}	$PF_3 + e = PF_2^{++} + 3e + F$	- 40	(LTB)	- 698
PF^{++}	$PF_3 + e = PF^{++} + 2F + 3e$	- 40	(LTB)	- 698

DISCUSSION OF RESULTS

(1) PF_3^+ $\qquad PF_3 + e = PF_3^+ + 2e$

The semilogarithmic method of Lossing, Tickner, and Bryce was considered to be the least subjective of the three methods used to determine the ionization potential of PF_3. For this reason, the 11.63 ±.02 e.v. value is taken as the "best" value for the ionization potential. However, the results of Humphries, Walsh, and Warsop[43] suggest that the appearance potential ought to be 11.7 e.v. or greater. For this reason, therefore, the Warren method value of 11.81 ±.06 e.v. cannot be completely disregarded. The Winters "energy difference distribution" procedure was found to the most subjective of the three methods, as the point of "disappearance" of the ΔI function was often somewhat arbitrary. Nevertheless, it is felt that the Winters method will yield excellent results in situations where the ion intensities can be measured to a high degree of precision.

Using 11.63 e.v., then, as the ionization potential of PF_3, and taking the heat of formation of PF_3 as -221.95 kilo-calories[42], the heat of formation of PF_3^+ is 46.1 kilo-calories.

(2) PF_2^+ $\qquad PF_3 + e = PF_2^+ + F + 2e$

The appearance potential of PF_2^+ was measured as 15.5 e.v. Therefore, $AP \geq IP(PF_2) + D(F_2P\text{-}F)$, where AP is the appearance potential, $IP(PF_2)$ is the ionization potential of PF_2, and $D(F_2P\text{-}F)$ is the dissociation energy of the $F_2P\text{-}F$ bond. The appearance potential can also be written $AP \geq IP(PF_3) + D^+(F_2P\text{-}F)$, where $D^+(F_2P\text{-}F)$ is

the dissociation energy of the F_2P^+-F bond. The average bond energy of the P-F bond is 5.1 e.v.[41], and if this can be taken as a crude estimation of $D(F_2P-F)$, then

$$IP(PF_2) \leqslant AP(PF_2^+) - 5.1$$
$$\leqslant 10.4 \text{ e.v.}$$

The upper limit on the ionization potential of PF_2 is quite reasonable as it would be expected to be less than the ionization potential of PF_3 (11.63), due to the fact that there are fewer electron withdrawing groups on PF_2. From the ionization potential of PF_3, it is also possible to calculate an upper limit on $D^+(F_2P-F)$ of 3.9 e.v.

The only other possible reaction to form PF_2^+ is

$$PF_3 + e = PF_2^+ + F^- + e$$

for which $AP \geqslant IP(PF_2) + D(F_2P-F) - EA(F)$, where EA(F) is the electron affinity of F^-. Taking EA(F) as 3.6 e.v.[50], then the $IP(PF_2)$ would have an upper limit of 14.0 e.v. This could conceivably put the IP of PF_2 over that of PF_3, which is highly unlikely. If this reaction were at all prevalent, moreover, a large ion current due to F^- would be expected as PF_2^+ is the most abundant ion in the mass spectrum. The fact that little F^- is formed indicates that this reaction is improbable.

(3) PF^+

(a) $PF_3 + e = PF^+ + 2F + 2e$

(b) $PF + e = PF^+ + 2e$

(c) $PF_2 + e = PF^+ + F + 2e$

From figure 28, it is evident from the shape of the ioniza-

tion efficiency curve that PF^+ is formed by two processes, one occuring at 20.5 e.v., and the other at 12.7 e.v. For reaction (a), the appearance potential can be written $AP \geq IP(PF) + D(F_2P\text{-}F) + D(FP\text{-}F)$. Assuming that $D(F_2P\text{-}F) = D(FP\text{-}F) = 5.1$ e.v., then $IP(PF) \leq 10.3$ e.v. Again, this is a reasonable value as the ionization potential of PF would be expected to be less than that of PF_2 or PF_3.

Other processes considered for the formation of PF^+ at 20.5 e.v. were

$$PF_3 + e = PF^+ + F + F^- + e$$
$$= PF^+ + 2F^-$$

However, these processes would put an upper limit on the ionization potential of about 14 and 17 e.v. respectively, which seems unreasonable as compared to the ionization potentials of PF_2 and PF_3.

For reaction (b) and (c), the PF_2 and PF would most likely be formed from the thermal decomposition of PF_3 on the filament. If reaction (b) were prevalent, then $IP(PF) \leq 12.7$, while if reaction (c) occurred, $IP(PF) \leq 7.6$. As it has already been established that $IP(PF) \leq 10.3$, if reaction (b) occurs, then at least 2.4 e.v. excess energy must be imparted to the PF^+ ion. As this is rather excessive for a single fragment to possess, reaction (c) is, perhaps, to be slightly favoured.

(4) P^+

(a) $PF_3 + e = P^+ + 3F + 2e$

(b) $PF + e = P^+ + F\ 2e$

(c) $P + e = P^+ + 2e$

From figure 26, P^+ is also formed from two different processes, one at 32.3 e.v. and one at -14 e.v. For reaction (a), the appearance

potential can be written AP = IP(P) + 3D(P-F). Using a value of 10.5 e.v. for the ionization potential of P^+ (16), the appearance potential would therefore be 25.8 e.v. Of all the possible processes, this corresponds the most closely to the experimental value of 32.3 e.v. Some other conceivable processes with their theoretical appearance potentials in brackets are:

$$PF_3 + e = P^+ + 2F + F^- + e \qquad (22.2)$$

$$= P^+ + F + 2F^- \qquad (18.3)$$

$$= P^+ + F^+ + 2F + 3e \qquad (42.9)$$

None of these reactions, however, are as close to the experimental appearance potential as reaction (a).

For the second process, two reactions are possible. Reaction (b) has a theoretical appearance potential of 15.6, while the theoretical appearance potential of reaction (c) is 10.5. Either of these reactions could occur, therefore, for the process at 14 e.v., reaction (b), perhaps, being slightly favoured.

(5) F^+

Several reactions can be considered for the formation of F^+ ions:

$$\text{(a)}\quad PF_3 + e = F^+ + PF_2 + 2e \qquad (22.7)$$

$$\text{(b)}\quad = F^+ + PF + F + 2e \qquad (27.7)$$

$$\text{(c)}\quad = F^+ + P + 2F + 2e \qquad (32.7)$$

$$\text{(d)}\quad = F^+ + P + 2F^- \qquad (36.0)$$

$$\text{(e)}\quad = F^+ + P + F + F^- + e \qquad (29.1)$$

As the appearance potential of F^+ is 36.0, reaction (d) would seem to be

favoured. However, reaction (c) cannot be discarded, especially since it occurs for compounds similar to PF_3 [51]. Reaction (c) is also favoured by the fact that the ion intensity for F^- is small, although it should be at least twice as large as F^+ if reaction (d) occurs.

(6) PF_3^{++} $PF_3 + e = PF_3^{++} + 3e$

The measured appearance potential for the peak at m/e 44 was 13.9 e.v. which corresponds closely with the ionization potential of CO_2 (13.8) [16]. Therefore, PF_3^{++} is almost certainly masked by the CO_2 background at low electron energies. As the mass of CO_2 is 43.9898 and the m/e value of PF_3^{++} is 43.9855, a resolution ($M/\Delta M$) of ten thousand would be required to split up the two peaks.

(7) F^-

As indicated in figure 29, F^- appears to be formed over a wide range of voltages at a very low intensity. As resonance capture processes occur only over a range of a few volts, if F^- is formed by electron-impact, then it would have to be by an ion pair-production reaction. However, this would involve breaking a P-F bond (5.1 e.v.) as well as the energy required to ionize the positive ion. The electron affinity of F (3.6 e.v.) is not enough to account for this energy, and therefore it would have to be provided by the ionizing electrons. A conceivable process in which only one P-F bond is broken and the positive ion has a relatively low appearance potential is:

$$PF + e = P^+ + F^- + e$$

The energy required for this reaction is 12.0 e.v. However, the F^- ion

is observed at energies well below this region (figure 29). The presence of F^- must therefore be accounted for by some other means than electron-impact; that is, the ion most likely arises from the decomposition of PF_3 on the filament. Once formed, the F^- ions would be drawn into the chamber by the electron-accelerating voltage, from which point they would be acted upon by the ion accelerating voltage and would appear in the mass spectrum. There seems to be no other explanation for the form of the ionization efficiency curve of F^-.

CONCLUSIONS

A. The ionization potential of PF_3 was measured as 11.63 $\pm$.02 (Lossing-Tickner-Bryce Method), 11.64 $\pm$.09 (Winters Method). and 11.81 $\pm$.06 (Warren Method) electron volts. The semi-logarithmic method of Lossing, Tickner, and Bryce was found to be the least subjective of the three methods used.

B. The appearance potentials of PF_2^+, PF^+, P^+, F^+, PF_2^{++}, and PF^+ were obtained and the heats of formation of PF_3^+, PF_2^+, P^+, PF_2^{++} and PF^{++} were calculated.

C. The probable reactions of dissociation of PF_3 were obtained from considerations of the Appearance Potentials. The origin of the F^- ion was not directly from electron-impact, but probably arises from the dissociation of PF_3 on the filament.

BIBLIOGRAPHY

BIBLIOGRAPHY

(1) Laidler, K. J. , "Reaction Kinetics", Vol. 1, MacMillan (1963)

(2) "Mass Spectral Data of the American Petroleum Institute", Research Project 44, serial no. 4, from Nat. Bur. of Standards

(3) Kiser, R. W., "Introduction to Mass Spectrometry and Its Applications", Prentice-Hall (1965)

(4) Beynon, J. H., "Mass Spectrometry" Elsevier (1960)

(5) Stevenson, D. P., 'Ion-Molecule Reactions' from "Mass Spectrometry", ed. C. A. McDowell, McGraw-Hill (1963)

(6) Coolidge, A. S., James, H. M., and Present, R. D., J. Chem. Phys. 4, 193 (1965)

(7) Sandorfy, C., "Electronic Spectra and Quantum Chemistry" Prentice-Hall (1964)

(8) Morrison, J. D., J. App. Phys. 28, 1409 (1957)

(9) Honig, R. E., J. Chem. Phys. 16, 105 (1948)

(10) Hickam, W. M., Fox, R. E., and Kjeldaas, T., Phys. Rev. 96,63 (1954)

(11) Stevenson, D. P., D. F. S. 10, 35 (1951)

(12) McDowell, C. A. and Warren, J. W., D.F.S. 10, 53 (1951)

(13) McDowell, C. A., 'The Ionization and Dissociation of Molecules' from "Mass Spectrometry" McGraw-Hill (1963)

(14) Morrison, J. D. and Stanton, H. E., J. Chem. Phys., 28, 9 (1958)

(15) Smyth, H. D., Proc. Roy. Soc., series A, 102, 283 (1922)

(16) Kiser, R. W., "Tables of Ionization Potentials", U.S. Atomic Energy Commision, Nat. Bur. of Standards

(17) Mitchel, J. J. and Colemann, F. F., J. Chem. Phys. 17, 44, (1949)

(18) Fox, R. E., Hickam, W. M., Kjeldaas, T., and Grove, D. J., Phys. Rev. 84, 859 (1951)

(19) Fox, R. E., Hickam, W. M., Grove, D. J., and Kjeldaas, T., Rev. Sci. Int 26, 1101 (1955)

(20) Marmet, P. and Kerwin, L., Can. J. Phys. 38, 787 + 942 (1960)

(21) Vought, R. H., Phys. Rev., 71, 93 (1947)

(22) Morrison, J. D., J. Chem. Phys. 19, 1305 (1951)

(23) Koffel, M. B., and Lad, R. A., J. Chem. Phys. 16, 420 (1948)

(24) Smith, P. T., Phys. Rev. 36, 1293 (1930)

(25) Stevenson, D. P. and Hipple, J. A., J.A.C.S. 64, 1305 (1951)

(26) Mariner, T. and Bleakney, W., Phys. Rev. 72, 792 + 807 (1947)

(27) Stevenson, D. P. and Hipple, J. A., Phys. Rev. 62, 237 (1942)

(28) Warren, J. W., Nature 165, 810 (1950)

(29) Field, F. H. and Franklyn, J. L., "Electron-Impact Phenomena" Academic, New York (1957)

(30) Lossing, F.P., Tickner, A. W., and Bryce, W. A., J. Chem. Phys. 19, 1254 (1951)

(31) Dibeler, V. H. and Reese, R. M., J. Res. Nat. Bur. of Standards 54, 127 (1955)

(32) Winters, R. E., Courchene, W. L., and Collins, J. H., Chem. and Eng. News, 44, June 6 (1966)

(33) Nicholson, A. J. C., J. Chem. Phys. 29, 1312 (1958)

(34) Hagstrum, H. D., Rev. Mod. Phys. 23, No. 3, 185 (1951)

(35) McCracken, D. D., "A Guide to Fortran Programing" Wiley (1965)

(36) Booth, H. S., and Bozarth, A. R., J.A.C.S. 61, 2927 (1939)

(37) Yost, D. M. and Anderson, T. F., J. Chem. Phys. 2, 624 (1934)

(38) Pauling, L. and Brockway, L. O., J.A.C.S. 57, 2684 (1936)

(39) Brockway, L. O. and Wall, F. T., J.A.C.S. 56, 2373 (1934)

(40) Bent, H. A. J.I.N.C. 19, 43 (1961)

(41) Neal, E. and Williams, L, T. D., J. Chem. Soc. 2485 (1955)

(42) Potter, R. L. and DiStephano, V. N., J. Phys. Chem. 65, 849 (1961)

(43) Humphries, C. M., Walsh, A. D., and Warsop, P. A., D.F.S. 35, 148 (1963)

(44) Muetterties, E. L., Bither, T. A., Farlow, M. W., and Coffmann, D. D., J.I.N.C. 16, 52 (1960)

(45) Hoffman, C. J., Inorg. Syn. 4, 149 (1953)

(46) Clark, R. J., Inorg. Chem. 3, No. 10, 1395 (1964)

(47) Clark, R. J. and Hoberman, P. I., Inorg. Chem. 4, No. 12, 1771 (1965)

(48) Williams, A. A., Inorg. Syn. 5, 95 (1957)

(49) Tullock, G. W. and Coffmann, D. D., J. Org. Chem. 25, 2016 (1960)

(50) Pritchard, H. O., Chem. Revs. 52, 537 (1953)

(51) Reese, R. M. and Dibeler, V. H., J. Chem. Phys. 24, No. 6, 1175 (1956)